Electromagnetic fields inside a large room with perfectly conducting walls

Research Report
ISSN 0167-9708
Coden: TEUEDE

Eindhoven
University of Technology
Netherlands

Faculty of Electrical Engineering

Electromagnetic Fields inside a Large Room with Perfectly Conducting Walls

by
G. Dolmans

EUT Report 95-E-286
ISBN 90-6144-286-9
March 1995

Eindhoven University of Technology Research Reports
EINDHOVEN UNIVERSITY OF TECHNOLOGY

Faculty of Electrical Engineering
Eindhoven The Netherlands

ISSN 0167-9708 Coden: TEUEDE

Electromagnetic Fields inside a Large Room with Perfectly Conducting Walls

by

G. Dolmans

EUT Report 95-E-286
ISBN 90-6144-286-9

EINDHOVEN
MARCH 1995

CIP-DATA KONINKLIJKE BIBLIOTHEEK, DEN HAAG

Dolmans, G.

Electromagnetic fields inside a large room with perfectly conducting walls / by G. Dolmans. - Eindhoven : Eindhoven University of Technology, Faculty of Electrical Engineering. - Fig. - (EUT report, ISSN 0167-9708; 95-E-286)
With ref.
ISBN 90-6144-286-9
NUGI 832
Subject headings: mobile radio systems / radiowave propagation / indoor communication

Electromagnetic fields inside a large room with perfectly conducting walls

G. Dolmans

Abstract

This EUT report describes the development of a model which can be used for the calculation of the electromagnetic fields inside a perfectly conducting cavity. A modal analysis has been chosen for the determination of the Green's functions inside the three dimensional enclosure. Using these Green's functions, the electromagnetic fields are calculated. The Green's functions have been written as double series, which are slowly convergent near the source coordinates.

Much attention is paid to the convergence properties of the series. It has been found that the convergence of the series is not only slow at the source coordinates but also at some other regions inside the cavity. An extraction technique has been used in order to improve the convergence properties of the Green's functions for a rectangular box cavity. Furthermore it has been shown that due to the presence of the multipath environment, the amplitudes of the electromagnetic fields change rapidly.

Keywords: mobile radio systems / radiowave propagation / indoor communication

Dolmans, G.
ELECTROMAGNETIC FIELDS INSIDE A LARGE ROOM WITH PERFECTLY CONDUCTING WALLS
Eindhoven: Faculty of Electrical Engineering, Eindhoven University of Technology,
The Netherlands, 1995.
EUT Report 95-E-286, ISBN 90-6144-286-9

Address of the author
Department of Electromagnetics
Faculty of Electrical Engineering, Eindhoven University of Technology
P.O. Box 513
5600 MB Eindhoven
The Netherlands

Acknowledgements

This research was supported by Philips Research Laboratories. The author wishes to thank Dr. M. Jeuken and Ir. L. Leyten for the helpful discussions.

Contents

Chapter 1

Introduction

Mobile communication systems have become very popular in the last years. New applications have been developed and antenna technology has made progress along with the advances in mobile communication systems [1]. In the past, antennas were developed independent of the rest of the equipment and the propagation environment. But in fact, the antenna, the equipment and the propagation environment are closely interrelated. Therefore factors related to propagation, equipment and environment conditions must be treated systematically when an antenna is designed.

There exists no theoretical electromagnetic framework for indoor propagation. The efforts on the latter subject are mainly directed towards measurements and statistical characterizations of the indoor channel [1]. Fujimoto [2] has noted that the general model for closed areas is very difficult to develop, because the field distribution in these environments is usually very complicated. He notes that there has been so far no positive action to define the field strength of such irregular fields.

In this report an attempt will be made to determine the field structure inside a closed cavity. Inside a real indoor environment, the electromagnetic waves will interact with objects (cabinets, desks etc.) and people which are moving around in the office. In this report we will restrict our analysis to an empty environment. The power levels and the polarisations of the electromagnetic fields inside the empty environment caused by a dipole antenna will be calculated. The walls, ceiling and floor of the indoor environment will be modeled as perfectly conducting. The geometry of this model is depicted by figure 1.1.

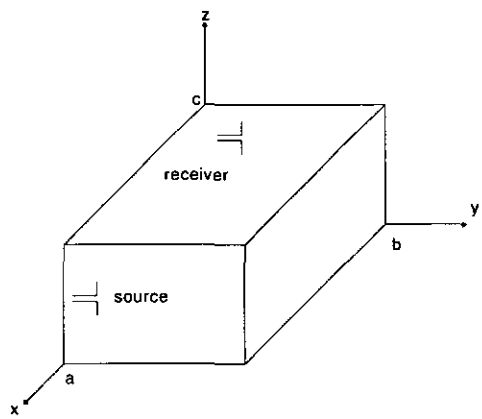

Figure 1.1: *Geometry of a rectangular box cavity*

The goal of this research is to develop a deterministic model which can be used for the prediction of the phases, strengths and polarisations of the electromagnetic fields inside an indoor environment. The information obtained by computing the electromagnetic fields can be used to evaluate the performance of the telecommunication link.

In the past many authors [3], [4] have done research on the determination of the electromagnetic fields inside a cavity resonator. The fields can be calculated by using a series expansion which is slowly convergent near the source coordinates. Bressan [8] has developed an extraction technique in order to accelerate the convergence of the series near the source coordinates. In this report the extraction technique will be used for the case of the rectangular box cavity. Furthermore it will be shown that much care must be taken by choosing which series will be used for the determination of the electromagnetic fields inside the cavity.

The structure of this report is as follows:
In chapter two the Green's functions inside a closed region have been presented. Green's functions are solutions of the electromagnetic fields caused by a point source, subjected to boundary conditions. The Green's functions inside the closed region have been written as triple series, which are related to the various possible modes inside the enclosure. The electromagnetic fields generated by an arbitrary source distribution can be calculated with the help of these Green's functions.

A specific case of a closed region is the rectangular box cavity. In chapter three, the Green's functions for this configuration are discussed. It has been shown that the Green's functions can be reduced to double series.

Chapter four focuses on the computation of the electromagnetic fields inside a cavity. The frequency of the electromagnetic waves is 2 GHz. Due to the reflections of the waves against the walls a multipath environment is created. It will be shown that there are many standing waves inside the cavity, so the amplitudes of the electromagnetic fields change rapidly. Much attention is paid to the convergence behaviour of the double series. It has been found that the convergence is not only slow at the singularities (observer near the source) but also at some other regions.

In order to accelerate the convergence of the Green's functions near the source coordinates, the Green's function has been divided into three parts, $\bar{\bar{G}}_1$, $\bar{\bar{G}}_2$ and $\bar{\bar{G}}_3$. The dyadics $\bar{\bar{G}}_1$ and $\bar{\bar{G}}_2$ contain the dominant singularity (like $\frac{1}{R^3}$) and the weaker singularity (like $\frac{1}{R}$), respectively. Unlike the original dyadic, the third dyadic $\bar{\bar{G}}_3$ is finite at the source coordinates. In chapter five an extraction technique has been used to improve the convergence properties of the series for a rectangular box cavity.

Some examples of the convergence behaviour for the Green's functions near the source coordinates are given in chapter six.

Chapter 2

Electromagnetic fields inside a perfectly conducting cavity

2.1 Introduction

In this chapter the electromagnetic fields inside a perfectly conducting cavity will be calculated. In the past a lot of research has been done for the determination of the free resonances occurring in a cavity (eigenvalue problem). The walls of the cavity are made of perfectly conducting material and the internal volume of the cavity consists of free space, so there are no losses and therefore many standing waves will build up inside the cavity.

In the following sections, the electromagnetic fields excited by an electric or magnetic source are calculated inside the cavity (source problem). The expressions describing the fields contain triple series, which are related to the various modes inside the cavity. Furthermore the formulae exist of volume integrals. The integrands of these volume integrals contain the volume currents weighted by the various eigenmodi. In section 2.3 the Green's functions of a cavity will be calculated. These Green's functions are an important tool for the determination of the electromagnetic field inside the closed region. A Green's function is the solution of the electromagnetic field excited by a point source. The fields inside the cavity generated by these point sources can be written as triple series. Finally, some remarks concerning the convergence behaviour of the various field expansions are given in section 2.4.

2.2 Eigenvector expansion of the electromagnetic field

A cavity surrounded by perfectly conducting walls is shown in figure 2.1.
$\vec{J}_e$ and $\vec{J}_m$ are the electric and magnetic current densities. S, V and $\vec{n}$ represent the surface of the cavity, the volume of the cavity and the unit outward normal to the surface S, respectively. The Maxwell's equations involving electric and magnetic sources can be written as

$$\begin{aligned}
&\nabla \times \vec{E} = -j\omega\mu_0\vec{H} - \vec{J}_m \quad \text{in V,} \\
&\nabla \times \vec{H} = j\omega\epsilon_0\vec{E} + \vec{J}_e \quad \text{in V,} \\
&\nabla.\vec{E} = \frac{\rho_e}{\epsilon_0} \quad \text{in V,} \\
&\nabla.\vec{H} = \frac{\rho_m}{\mu_0} \quad \text{in V,}
\end{aligned} \tag{2.1}$$

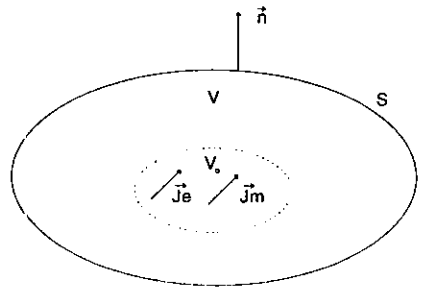

Figure 2.1: *Arbitrary cavity containing electric and magnetic sources*

where we have assumed a time-harmonic dependence of the form $e^{j\omega t}$, ω is the radial frequency. $\vec{E}$, $\vec{H}$ are the electric and magnetic fields, respectively. The electric and magnetic charge densities are represented by ρ_e and ρ_m. The charges and current densities are the sources for the electric and magnetic fields. The volume inside the cavity consists of free space with permeability μ_0 and permittivity ϵ_0, respectively. Outside the volume V_o the cavity contains no sources, so the source free Maxwell's equations can be used in this particular area. The necessary boundary condition is given by

$$\vec{n} \times \vec{E} = \vec{0} \quad \text{on} \quad \text{S}. \tag{2.2}$$

The vector wave equations can be obtained by taking the curl of the first two equations in (2.1):

$$\begin{aligned} \nabla \times \nabla \times \vec{E} - k_0^2 \vec{E} &= -j\omega\mu_0 \vec{J}_e - \nabla \times \vec{J}_m, \\ \nabla \times \nabla \times \vec{H} - k_0^2 \vec{H} &= -j\omega\epsilon_0 \vec{J}_m + \nabla \times \vec{J}_e, \end{aligned} \tag{2.3}$$

where $k_0 = \omega\sqrt{\epsilon_0\mu_0}$ denotes the free space wavenumber. A modal analysis will be used for the determination of the electric and magnetic fields inside a cavity. This method is described by Collin [4] and Van Bladel [9]. Using this modal analysis, the electromagnetic field can be written as an expansion of the empty cavity eigenmodes. The eigenmodes are the solution of the source-free Maxwell's equations and the relevant boundary conditions. From vector calculus it is known that a vector function is uniquely determined by its curl and divergence. This means that an arbitrary continuous vector field can be expressed in terms of the gradient of a scalar function and the curl of a vector function. Thus an arbitrary field inside a cavity can be presented by solenoidal (divergenceless) and irrotational (zero curl) eigenmodes.

Numerous workers have studied the problem of representing the electric or magnetic field in terms of their eigenfunction representation. Collin [4], [5] has noted that the electromagnetic field inside a cavity cannot be presented by solenoidal modes only. His conclusion was that an additional term is needed in order that the condition $\nabla.\vec{E} = \rho_e/\epsilon_o$ will be satisfied. Consequently, to derive a complete solution that is valid in both the source and source-free regions of the cavity, an additional non-divergenceless term must be included in the expansion [6], [3], [7].
Using these conclusions, the electric and magnetic fields inside a cavity can be written as

$$\begin{aligned} \vec{E} &= \sum_{r=0}^{\infty}\sum_{s=0}^{\infty}\sum_{t=0}^{\infty} A_{rst}\vec{E}_{rst} + B_{rst}\vec{L}_{rst}, \\ \vec{H} &= \sum_{r=0}^{\infty}\sum_{s=0}^{\infty}\sum_{t=0}^{\infty} C_{rst}\vec{H}_{rst} + D_{rst}\vec{K}_{rst}, \end{aligned} \tag{2.4}$$

where A_{rst} and B_{rst} represent the amplitude coefficients of the orthonormal solenoidal $\vec{E}_{rst}$ and orthonormal irrotational $\vec{L}_{rst}$ eigenmodes. C_{rst} and D_{rst} are the amplitude coefficients of the orthonormal solenoidal $\vec{H}_{rst}$ and orthonormal irrotational $\vec{K}_{rst}$ modes.

In numerical solutions only finite summations can be evaluated. The eigenfunctions will be ordered in such a way that the lower order eigenfunctions are smoother than the higher order eigenfunctions. If the function represented by an expansion of eigenfunctions (in this case the electric and magnetic field) oscillates slowly, only a few eigenfunctions are needed. This is the reason that in practice the electromagnetic fields can be calculated by a finite number of eigenfunctions.
First the properties of the eigenmodes will be discussed. As mentioned earlier, the eigenmodes are the solution of the source-free Maxwell's equations subjected to the relevant boundary conditions:

$$\begin{aligned} &\nabla \times \vec{F}_{rst} = -j\omega_{rst}\mu_0\vec{G}_{rst} && \text{in V,} \\ &\nabla \times \vec{G}_{rst} = j\omega_{rst}\epsilon_0\vec{F}_{rst} && \text{in V,} \\ &\vec{n} \times \vec{F}_{rst} = \vec{0} && \text{on S,} \end{aligned} \tag{2.5}$$

where $\vec{F}_{rst}$ and $\vec{G}_{rst}$ are eigenvectors representing the electric and magnetic field, respectively. The radial resonance frequency is denoted by the symbol ω_{rst}. Taking the curl of the above equations, the following wave equations are obtained

$$\begin{aligned} &\nabla \times \nabla \times \vec{F}_{rst} - k_{rst}^2\vec{F}_{rst} = \vec{0}, \\ &\nabla \times \nabla \times \vec{G}_{rst} - k_{rst}^2\vec{G}_{rst} = \vec{0}, \end{aligned} \tag{2.6}$$

where $k_{rst} = \sqrt{\omega_{rst}^2\epsilon_0\mu_0}$ represents the three dimensional wavenumber of the cavity.
The solenoidal eigenmodes $\vec{E}_{rst}$ used for the expansion of the electric field have the following properties

$$\begin{aligned} &(\nabla^2 + k_{rst}^2)\vec{E}_{rst} = \vec{0} && \text{in V,} \\ &\nabla.\vec{E}_{rst} = 0 && \text{in V,} \\ &\vec{n} \times \vec{E}_{rst} = \vec{0} && \text{on S.} \end{aligned} \tag{2.7}$$

These solenoidal eigenfunctions $\vec{E}_{rst}$ can be obtained from scalar functions [7]. Because the electric eigenmodes $\vec{L}_{rst}$ are irrotational, the functions $\vec{L}_{rst}$ lie in the null space of the $\nabla \times \nabla \times$ operator [4]. Therefore another method will be used for the determination of the irrotational functions. Using a scalar Helmholtz equation, the irrotational functions can be generated from the gradient of the scalar function ϕ_{rst}

$$\begin{aligned} &(\nabla^2 + l_{rst}^2)\phi_{rst} = 0 && \text{in V,} \\ &l_{rst}\vec{L}_{rst} = \nabla\phi_{rst} && \text{in V,} \\ &\nabla \times \vec{L}_{rst} = \vec{0} && \text{in V,} \\ &\vec{n} \times \vec{L}_{rst} = \vec{0} && \text{on S.} \end{aligned} \tag{2.8}$$

The wavenumbers k_{rst} and l_{rst} will be equal for a rectangular cavity. The same method will be applied to the magnetic eigenmodes, the solenoidal magnetic eigenmodes $\vec{H}_{rst}$ are given by

$$\begin{aligned} &(\nabla^2 + k_{rst}^2)\vec{H}_{rst} = \vec{0} && \text{in} \quad \text{V}, \\ &\nabla.\vec{H}_{rst} = 0 && \text{in} \quad \text{V}, \\ &\vec{n}.\vec{H}_{rst} = 0 && \text{on} \quad \text{S}. \end{aligned} \tag{2.9}$$

The irrotational magnetic eigenmodes $\vec{K}_{rst}$ are given by

$$\begin{aligned} &(\nabla^2 + l_{rst}^2)\psi_{rst} = 0 && \text{in} \quad \text{V}, \\ &l_{rst}\vec{K}_{rst} = \nabla\psi_{rst} && \text{in} \quad \text{V}, \\ &\nabla \times \vec{K}_{rst} = \vec{0} && \text{in} \quad \text{V}, \\ &\vec{n}.\vec{K}_{rst} = 0 && \text{on} \quad \text{S}. \end{aligned} \tag{2.10}$$

The coefficients A_{rst}, B_{rst} , C_{rst} and D_{rst} of the eigenfunctions can be calculated by using the Maxwell's equations and the orthonormal properties of the eigenfunctions. Multiplying the second Maxwell equation with the scalar $j\omega\mu_0$ and taking the scalar product with the eigenmode $\vec{E}_{rst}$ results in

$$j\omega\mu_0\vec{E}_{rst}.\left(\nabla \times \vec{H}\right) = -k_0^2\left(\vec{E}.\vec{E}_{rst}\right) + j\omega\mu_0\left(\vec{J}_e.\vec{E}_{rst}\right). \tag{2.11}$$

Multiplying the second source-free Maxwell's equation of the eigenmodes with the same scalar and taking the scalar product with the electric field $\vec{E}$ gives

$$j\omega_{rst}\mu_0\vec{E}.\left(\nabla \times \vec{H}_{rst}\right) = -k_{rst}^2\left(\vec{E}.\vec{E}_{rst}\right). \tag{2.12}$$

Subtraction of these equations and using Maxwell's equations results in

$$\begin{aligned} &\vec{E}.(\nabla \times \nabla \times \vec{E}_{rst}) - \vec{E}_{rst}.(\nabla \times \nabla \times \vec{E}) = \\ &(k_{rst}^2 - k_0^2)(\vec{E}.\vec{E}_{rst}) + j\omega\mu_0(\vec{J}_e.\vec{E}_{rst}) \end{aligned} \tag{2.13}$$

The following relationship will be used [7]

$$\begin{aligned} &\int\int\int_V \vec{E}.(\nabla \times \nabla \times \vec{E}_{rst}) - \vec{E}_{rst}.(\nabla \times \nabla \times \vec{E})\, dV = \\ &\int\int_S (\vec{E}_{rst} \times \nabla \times \vec{E} - \vec{E} \times \nabla \times \vec{E}_{rst}).\vec{n}\, dS \end{aligned} \tag{2.14}$$

Using equation (2.14) and the boundary conditions on the surface S results in

$$\int\int\int_V \left(k_{rst}^2 - k_0^2\right)\left(\vec{E}.\vec{E}_{rst}\right) + j\omega\mu_0\left(\vec{J}_e.\vec{E}_{rst}\right) dV = 0. \tag{2.15}$$

The previous equation can be written as

$$\int\int\int \vec{E}.\vec{E}_{rst} dV = \frac{-j\omega\mu_0 \int\int\int \vec{J}_e.\vec{E}_{rst} dV}{k_{rst}^2 - k_0^2}. \tag{2.16}$$

The orthonormal properties of the eigenmodes $\vec{E}_{rst}$ are represented by the following equation

$$\int\int\int \vec{E}_{1rst}.\vec{E}_{2rst}dV = \delta_{rst}, \tag{2.17}$$

where $\vec{E}_{1rst}$ and $\vec{E}_{2rst}$ are two solutions of the free-space wave equation (2.6). The kronecker symbol δ_{rst} equals unity when $r = s = t$. The kronecker symbol equals zero otherwise. Using the formula of the expansion of the electric field (2.4) and the orthonormal properties of the eigenvectors results in

$$A_{rst} = \frac{-j\omega\mu_0}{k_{rst}^2 - k_0^2}\int\int\int \vec{J}_e.\vec{E}_{rst}dV. \tag{2.18}$$

A similar procedure can be followed for the calculation of the amplitude coefficients B_{rst}, C_{rst} and D_{rst}. Detailed proofs of the orthogonality properties of the various eigenmodes can be found in [4] and [11]. The expansion of the electric field can be written as

$$\begin{aligned}\vec{E} &= -j\omega\mu_0 \sum_{r=0}^{\infty}\sum_{s=0}^{\infty}\sum_{t=0}^{\infty}\frac{\vec{E}_{rst}}{k_{rst}^2 - k_0^2}\int\int\int_V \vec{J}_e.\vec{E}_{rst}dV \\ &\quad +j\omega\mu_0 \sum_{r=0}^{\infty}\sum_{s=0}^{\infty}\sum_{t=0}^{\infty}\frac{\vec{L}_{rst}}{k_0^2}\int\int\int_V \vec{J}_e.\vec{L}_{rst}dV \\ &\quad - \sum_{r=0}^{\infty}\sum_{s=0}^{\infty}\sum_{t=0}^{\infty}\frac{k_{rst}}{k_{rst}^2 - k_0^2}\vec{E}_{rst}\int\int\int_V \vec{J}_m.\vec{H}_{rst}dV.\end{aligned} \tag{2.19}$$

The magnetic solenoidal eigenmodes $\vec{H}_{rst}$ are related to the electric solenoidal eigenmodes $\vec{E}_{rst}$ by the equation

$$\vec{H}_{rst} = \frac{1}{k_{rst}}\nabla \times \vec{E}_{rst}. \tag{2.20}$$

The magnetic field $\vec{H}(\vec{r})$ can be expanded in a similar way

$$\begin{aligned}\vec{H} &= -j\omega\epsilon_0 \sum_{r=0}^{\infty}\sum_{s=0}^{\infty}\sum_{t=0}^{\infty}\frac{1}{k_{rst}^2 - k_0^2}\vec{H}_{rst}\int\int\int_V \vec{J}_m.\vec{H}_{rst}dV \\ &\quad +j\omega\epsilon_0 \sum_{r=0}^{\infty}\sum_{s=0}^{\infty}\sum_{t=0}^{\infty}\frac{\vec{K}_{rst}}{k_0^2}\int\int\int_V \vec{J}_m.\vec{K}_{rst}dV \\ &\quad + \sum_{r=0}^{\infty}\sum_{s=0}^{\infty}\sum_{t=0}^{\infty}\frac{k_{rst}}{k_{rst}^2 - k_0^2}\vec{H}_{rst}\int\int\int_V \vec{J}_e.\vec{E}_{rst}dV.\end{aligned} \tag{2.21}$$

2.3 Eigenvector expansion of the Green's functions

At this point the electromagnetic fields are expressed in terms of eigenvectors involving an arbitrary electric or magnetic source. The strengths of the sources determine the amplitude coefficients A_{rst}, B_{rst}, C_{rst} and D_{rst}. These coefficients are calculated by using a volume integral.

Another way to solve the problem is to calculate the expansions of the fields due to an elementary source. The solution of the electromagnetic field excited by a point source is called Green's function. The Green's function method makes use of delta functions. A delta function is not a function in common sense. One must be careful when taking derivatives of the delta function, these derivatives must be specified in the distributional sense. The general solution (arbitrary source) can be written as a superposition of the effects of the elementary sources at various locations [10].

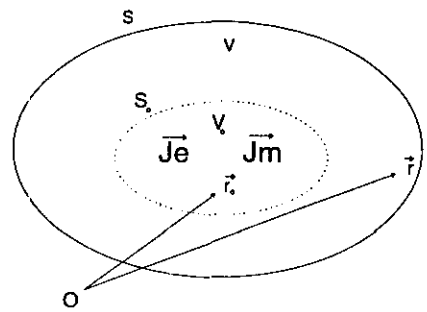

Figure 2.2: *Coordinate system*

The coordinate system used by the calculation of the Green's function is drawn in figure 2.2. S_o and V_o are the surface boundary and the volume which contains the sources. The source coordinates and the field coordinates are denoted by $\vec{r}_o$ and $\vec{r}$. The electric field caused by an elementary electric current source is represented by the dyadic $\bar{\bar{G}}_e^1$

$$\nabla \times \nabla \times \bar{\bar{G}}_e^1 - k_0^2 \ \bar{\bar{G}}_e^1 = \delta(\vec{r} - \vec{r}_o)\, \bar{\bar{I}}, \tag{2.22}$$

$$\vec{n} \times \bar{\bar{G}}_e^1 = \bar{\bar{0}}, \tag{2.23}$$

where $\bar{\bar{I}}$ and $\bar{\bar{0}}$ are the unit dyadic and the zero dyadic, respectively. The magnetic field caused by an elementary magnetic current source is given by the following wave equation

$$\nabla \times \nabla \times \bar{\bar{G}}_m^1 - k_0^2 \ \bar{\bar{G}}_m^1 = \delta(\vec{r} - \vec{r}_o)\, \bar{\bar{I}}, \tag{2.24}$$

$$\vec{n}.\ \bar{\bar{G}}_m^1 = \vec{0}. \tag{2.25}$$

A vector can be presented by a tensor of rank one. In a similar way a dyadic is a tensor of rank two. The dyadic has nine tensor components, each of which is a scalar. So the dyadic can be expressed in terms of scalars and unit vectors as follows

$$\begin{aligned} \bar{\bar{G}} &= G_{xx}\vec{e}_x\vec{e}_x + G_{xy}\vec{e}_x\vec{e}_y + G_{xz}\vec{e}_x\vec{e}_z \\ &+ G_{yx}\vec{e}_y\vec{e}_x + G_{yy}\vec{e}_y\vec{e}_y + G_{yz}\vec{e}_y\vec{e}_z \\ &+ G_{zx}\vec{e}_z\vec{e}_x + G_{zy}\vec{e}_z\vec{e}_y + G_{zz}\vec{e}_z\vec{e}_z \end{aligned} \tag{2.26}$$

where the quantities G_{ij} are scalars. This representation of a dyadic will be used frequently in this report. When the solution for the unit source is known, the solution for an arbitrary source distribution follows by superposition. Using this concept, the electric field can be written as

$$\vec{E}(\vec{r}) = -j\omega\mu_0 \int\int\int_{V_o} \bar{\bar{G}}_e^1(\vec{r},\vec{r}_o).\vec{J}_e(\vec{r}_o)dV_o - \int\int\int_{V_o} \bar{\bar{G}}_m^2(\vec{r},\vec{r}_o).\vec{J}_m(\vec{r}_o)dV_o. \tag{2.27}$$

Also the magnetic field caused by an arbitrary source distribution follows by superposition. The magnetic field is given by

$$\vec{H}(\vec{r}) = -j\omega\epsilon_0 \int\int\int_{V_o} \bar{\bar{G}}_m^1(\vec{r},\vec{r}_o).\vec{J}_m(\vec{r}_o)dV_o + \int\int\int_{V_o} \bar{\bar{G}}_e^2(\vec{r},\vec{r}_o).\vec{J}_e(\vec{r}_o)dV_o. \tag{2.28}$$

The algebra of dyadics has a very close correspondence with matrix algebra. Therefore in literature, the electric Green's functions are often written in a matrix form:

$$\bar{\bar{G}}_e^i = \begin{bmatrix} G_{exx}^i & G_{exy}^i & G_{exz}^i \\ G_{eyx}^i & G_{eyy}^i & G_{eyz}^i \\ G_{ezx}^i & G_{ezy}^i & G_{ezz}^i \end{bmatrix}, \tag{2.29}$$

where i=1,2. The magnetic Green's functions are given by

$$\bar{\bar{G}}_m^i = \begin{bmatrix} G_{mxx}^i & G_{mxy}^i & G_{mxz}^i \\ G_{myx}^i & G_{myy}^i & G_{myz}^i \\ G_{mzx}^i & G_{mzy}^i & G_{mzz}^i \end{bmatrix}, \tag{2.30}$$

where i=1,2. Using the results of the modal analysis (2.19) , the Green's functions of the electric field can be written as

$$\begin{aligned} \bar{\bar{G}}_e^1 &= \sum_{r=0}^{\infty}\sum_{s=0}^{\infty}\sum_{t=0}^{\infty} \frac{\vec{E}_{rst}(\vec{r})\vec{E}_{rst}(\vec{r}_o)}{k_{rst}^2 - k_0^2} - \frac{1}{k_0^2}\sum_{r=0}^{\infty}\sum_{s=0}^{\infty}\sum_{t=0}^{\infty}\vec{L}_{rst}(\vec{r})\vec{L}_{rst}(\vec{r}_o), \\ \bar{\bar{G}}_m^2 &= \sum_{r=0}^{\infty}\sum_{s=0}^{\infty}\sum_{t=0}^{\infty} \frac{k_{rst}\vec{E}_{rst}(\vec{r})\vec{H}_{rst}(\vec{r}_o)}{k_{rst}^2 - k_0^2}. \end{aligned} \tag{2.31}$$

Using (2.21), the Green's functions of the magnetic field can be written as

$$\begin{aligned} \bar{\bar{G}}_m^1 &= \sum_{r=0}^{\infty}\sum_{s=0}^{\infty}\sum_{t=0}^{\infty} \frac{\vec{H}_{rst}(\vec{r})\vec{H}_{rst}(\vec{r}_o)}{k_{rst}^2 - k_0^2} - \frac{1}{k_0^2}\sum_{r=0}^{\infty}\sum_{s=0}^{\infty}\sum_{t=0}^{\infty}\vec{K}_{rst}(\vec{r})\vec{K}_{rst}(\vec{r}_o), \\ \bar{\bar{G}}_e^2 &= \sum_{r=0}^{\infty}\sum_{s=0}^{\infty}\sum_{t=0}^{\infty} \frac{k_{rst}\vec{H}_{rst}(\vec{r})\vec{E}_{rst}(\vec{r}_o)}{k_{rst}^2 - k_0^2}. \end{aligned} \tag{2.32}$$

2.4 Alternative Green's functions and convergence properties

At this point the electric and magnetic field excited by an elementary source can be calculated when the geometry of the boundary is given. The electric and magnetic field due to an arbitrary source can be calculated by using the equations (2.27) and (2.28). Collin [4] has shown that outside the source region ($\vec{r} \neq \vec{r}_o$) the Green's functions are completely described with solenoidal eigenfunctions. Yaghjian [12] has given a rigorous mathematical theory which calculates a generalized Green's function valid inside as well as outside the source region without using the irrotational eigenvectors. Using these generalized Green's functions, the electric and magnetic fields are given by

$$\vec{E}(\vec{r}) = -j\omega\mu_0 \lim_{\delta\to 0} \int\int\int_{V_o - V_\delta} \bar{\bar{G}}_e^{1*}(\vec{r},\vec{r}_o).\vec{J}_e(\vec{r}_o)dV_o - \frac{\bar{\bar{L}}_1.\vec{J}_e(\vec{r})}{j\omega\epsilon_0} - \tag{2.33}$$

$$\int\int\int_{V_o} \bar{\bar{G}}_m^2(\vec{r},\vec{r}_o).\vec{J}_m(\vec{r}_o)dV_o,$$

$$\vec{H}(\vec{r}) = -j\omega\epsilon_0 \lim_{\delta\to 0} \int\int\int_{V_o - V_\delta} \bar{\bar{G}}_m^{1*}(\vec{r},\vec{r}_o).\vec{J}_m(\vec{r}_o)dV_o - \frac{\bar{\bar{L}}_2.\vec{J}_m(\vec{r})}{j\omega\mu_0} + \tag{2.34}$$

$$\int\int\int_{V_o} \bar{\bar{G}}_e^2(\vec{r},\vec{r}_o).\vec{J}_e(\vec{r}_o)dV_o.$$

The source dyadics $\bar{\bar{L}}_1$ and $\bar{\bar{L}}_2$ (not to be confused with the irrotational eigenvector $\vec{L}$) are related to the geometry of the principal volume V_δ. The electric or magnetic source is located inside this principal volume V_δ. Using a pillbox of arbitrary cross-section with a $\vec{e_z}$ -axis for the principal volume V_δ, the two source dyadics are given by

$$\bar{\bar{L}}_1 = \bar{\bar{L}}_2 = \vec{e}_z \vec{e}_z. \tag{2.35}$$

The pillbox is shown in figure 2.3.

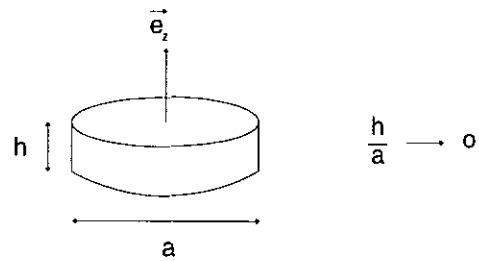

Figure 2.3: *Pill box*

The two generalized Green's functions $\bar{\bar{G}}_e^{I*}$ and $\bar{\bar{G}}_m^{I*}$ can be written as expansions of solenoidal eigenvectors [4], [13]:

$$\begin{aligned} \bar{\bar{G}}_e^{I*} &= \sum_{r=0}^{\infty}\sum_{s=0}^{\infty}\sum_{t=0}^{\infty} \frac{k_{rst}^2 \vec{E}_{rst}(\vec{r})\vec{E}_{rst}(\vec{r}_o)}{k_0^2(k_{rst}^2 - k_0^2)}, \\ \bar{\bar{G}}_m^{I*} &= \sum_{r=0}^{\infty}\sum_{s=0}^{\infty}\sum_{t=0}^{\infty} \frac{k_{rst}^2 \vec{H}_{rst}(\vec{r})\vec{H}_{rst}(\vec{r}_o)}{k_0^2(k_{rst}^2 - k_0^2)}, \end{aligned} \tag{2.36}$$

So there are two representations of the electromagnetic fields inside a cavity. The first one is given by the equations (2.27), (2.28), (2.31) and (2.32). This expansion uses irrotational eigenvectors. The second type of expansion is given by the equations (2.33), (2.34) and (2.36). The second expansion does not contain irrotational eigenmodes, however, an additional term $\bar{\bar{L}}.\vec{J}$ is needed to calculate the electromagnetic fields inside the cavity.

To make a choice between these two expansions, it is important to evaluate the convergence of these expansions. Omar, et. al. [13] have pointed out that in case of surface or filamentary currents, the terms $\frac{\vec{J}_e}{j\omega\epsilon_0}$ and $\frac{\vec{J}_m}{j\omega\mu_0}$ have dirac-delta dependencies. The electromagnetic fields must be continuous in the cavity, this means that a part of the series must compensate the dirac-delta dependence. When the generalized Green's functions $\bar{\bar{G}}_e^{I*}$ and $\bar{\bar{G}}_m^{I*}$ are used for the calculation of the electromagnetic fields, the series do not converge very well near or at the source coordinates. The series converge only well if the source is a volume-distribution. It is advisable to use the pure solenoidal expansion for the calculation of the electromagnetic fields when the source consists of a volume-distribution current. In this report electric and magnetic dipoles will be used, therefore the expansions using the solenoidal and the irrotational modes are chosen.

In this section the Green's functions are described by using triple series. In the following sections one series is calculated in closed form, so the Green's functions are given by double series. The above conclusions are only valid when the Green's function's are described by triple series.

2.5 Conclusions

In this chapter we have determined the electromagnetic fields caused by an elementary electric or magnetic source inside a closed region. One way to calculate these fields is the use of Green's functions. A Green's function is an important tool for the solution of electromagnetic problems. Because we deal with a three dimensional problem, the Green's functions are written as triple series containing the eigenmodes of the cavity. In literature, many representations for the Green's functions exist, therefore some remarks are made concerning the convergence behaviour of these different Green's functions in section 2.4.

The theory presented in this chapter will be used for the calculation of the electromagnetic fields inside a rectangular box cavity.

Chapter 3

Eigenvectors of a rectangular box cavity

3.1 Introduction

In section 3.2 the four Green's dyadics of a rectangular box cavity will be developed. The electromagnetic fields caused by an electric or magnetic source are completely described by these four Green's dyadics. Using the analysis described in chapter two, the Green's functions can be represented by triple series of solenoidal and irrotational modes [3] [14]. These modes will be calculated using vector calculus on four scalar functions. The necessary computational time can be reduced by calculating one of the three series in closed form. Because we can arbitrary choose which variable (r, s or t) will be used, alternative representations can be obtained for the Green's functions. This is an advantage of the eigenfunction method, because we can now choose the representation with the best numerical convergence behaviour in the region under consideration. The various expressions for the Green's functions will be compared with each other in chapter four.

3.2 Eigenvectors of a rectangular cavity

The rectangular box cavity and the coordinate system are shown in the following figure:

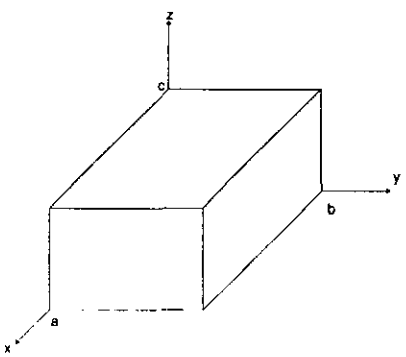

Figure 3.1: *Rectangular box cavity*

The dimensions of the cavity in the x -,y - and z -directions are denoted by a, b, and c, respectively. The source coordinates of an electric or magnetic source are given by (x_o, y_o, z_o) and the field coordinates are represented by (x, y, z).

The complete set of solenoidal electric eigenvectors $\vec{E}_{rst}$ can be found by using two scalar functions. These scalars will be chosen in such a way that the boundary conditions have been fulfilled.

Furthermore the eigenvectors must be independent and mutually orthogonal solutions of the vector wave equation.

One scalar function for a rectangular cavity is given by

$$\Psi_{rst} = \left[\left(\frac{r\pi}{a}\right)^2 + \left(\frac{s\pi}{b}\right)^2\right]^{-\frac{1}{2}} \left(\frac{\epsilon_{or}\epsilon_{os}\epsilon_{ot}}{abc}\right)^{\frac{1}{2}} \cos\frac{r\pi x}{a} \cos\frac{s\pi y}{b} \sin\frac{t\pi z}{c}, \tag{3.1}$$

where ϵ_{or}, ϵ_{os} and ϵ_{ot} are the Neumann factors, which equal unity for $r = 0$, $s = 0$ and $t = 0$, respectively. These factors equal two otherwise. The first set of solenoidal modes $\vec{M}_{rst}$ is given by

$$\vec{M}_{rst} = \nabla \times (\Psi_{rst}\vec{e}_z), \tag{3.2}$$

where $\vec{e}_z$ is the unit vector into the z-direction. The second set of solenoidal modes $\vec{N}_{rst}$ is obtained from the second scalar function

$$\Phi_{rst} = \left[\left(\frac{r\pi}{a}\right)^2 + \left(\frac{s\pi}{b}\right)^2\right]^{-\frac{1}{2}} \left(\frac{\epsilon_{or}\epsilon_{os}\epsilon_{ot}}{abc}\right)^{\frac{1}{2}} \sin\frac{r\pi x}{a} \sin\frac{s\pi y}{b} \cos\frac{t\pi z}{c}, \tag{3.3}$$

$$k_{rst}\vec{N}_{rst} = \nabla \times \nabla \times (\Phi_{rst}\vec{e}_z), \tag{3.4}$$

where the three dimensional wavenumber k_{rst} is given by

$$k_{rst} = \sqrt{\left(\frac{r\pi}{a}\right)^2 + \left(\frac{s\pi}{b}\right)^2 + \left(\frac{t\pi}{c}\right)^2}. \tag{3.5}$$

Now the complete set of solenoidal electric modes $\vec{E}_{rst} \in \left\{\vec{M}_{rst}, \vec{N}_{rst}\right\}$ has been derived for the case of a rectangular box cavity. The irrotational electric modes $\vec{L}_{rst}$ are given by

$$\begin{aligned} \Upsilon_{rst} &= \left(\frac{\epsilon_{or}\epsilon_{os}\epsilon_{ot}}{abc}\right)^{\frac{1}{2}} \sin\frac{r\pi x}{a} \sin\frac{s\pi y}{b} \sin\frac{t\pi z}{c}, \\ k_{rst}\vec{L}_{rst} &= \nabla\Upsilon_{rst}. \end{aligned} \tag{3.6}$$

Note that the use of the irrotational functions was needed in order to derive the electromagnetic field in the source region. However, these irrotational functions are responsible not only for the field in the source region but also contributes to the electric field in a source-free region [3].

In the previous chapter the magnetic eigenvectors $\vec{H}_{rst}$ and $\vec{K}_{rst}$ were also needed for the calculation of the electromagnetic field. Notice that the solenoidal magnetic eigenvectors can be found by using the following equation

$$k_{rst}\vec{H}_{rst} = \nabla \times \vec{E}_{rst}. \tag{3.7}$$

The irrotational magnetic eigenvectors are given by

$$\begin{aligned} \Omega_{rst} &= \left(\frac{\epsilon_{or}\epsilon_{os}\epsilon_{ot}}{abc}\right)^{\frac{1}{2}} \cos\frac{r\pi x}{a} \cos\frac{s\pi y}{b} \cos\frac{t\pi z}{c}, \\ k_{rst}\vec{K}_{rst} &= \nabla\Omega_{rst}. \end{aligned} \tag{3.8}$$

In chapter two, solenoidal and irrotational eigenvectors are chosen for the representation of the electromagnetic fields inside a perfectly conducting cavity. The Green's functions used for the expansion of the electric field are given by

$$\begin{aligned}\bar{\bar{G}}_e^1 &= \sum_{r=0}^{\infty}\sum_{s=0}^{\infty}\sum_{t=0}^{\infty}\frac{\vec{E}_{rst}(\vec{r})\vec{E}_{rst}(\vec{r}_o)}{k_{rst}^2-k_0^2}-\frac{1}{k_0^2}\sum_{r=0}^{\infty}\sum_{s=0}^{\infty}\sum_{t=0}^{\infty}\vec{L}_{rst}(\vec{r})\vec{L}_{rst}(\vec{r}_o),\\ \bar{\bar{G}}_m^2 &= \sum_{r=0}^{\infty}\sum_{s=0}^{\infty}\sum_{t=0}^{\infty}\frac{k_{rst}\vec{E}_{rst}(\vec{r})\vec{H}_{rst}(\vec{r}_o)}{k_{rst}^2-k_0^2}.\end{aligned} \tag{3.9}$$

So these Green's functions representing the electric field are known by means of calculating three eigenvectors $\vec{E}_{rst}$, $\vec{L}_{rst}$ and $\vec{H}_{rst}$. As mentioned earlier, the eigenvectors are calculated using vector operations on the scalar functions Ψ_{rst}, Φ_{rst} and Υ_{rst}. Performing these operations, the first electric Green's function can be written as

$$\begin{aligned}\bar{\bar{G}}_e^1(\vec{r},\vec{r}_o) \;=\; & \sum_{r=0}^{\infty}\sum_{s=0}^{\infty}\sum_{t=0}^{\infty}\frac{\epsilon_{or}\epsilon_{os}\epsilon_{ot}}{abc\left(k_{rst}^2-k_0^2\right)k_0^2}\\ & \left[\left[k_0^2-\left(\frac{r\pi}{a}\right)^2\right]\cos\frac{r\pi x}{a}\cos\frac{r\pi x_o}{a}\sin\frac{s\pi y}{b}\sin\frac{s\pi y_o}{b}\sin\frac{t\pi z}{c}\sin\frac{t\pi z_o}{c}\vec{e}_x\vec{e}_x\right.\\ & +\left[k_0^2-\left(\frac{s\pi}{b}\right)^2\right]\sin\frac{r\pi x}{a}\sin\frac{r\pi x_o}{a}\cos\frac{s\pi y}{b}\cos\frac{s\pi y_o}{b}\sin\frac{t\pi z}{c}\sin\frac{t\pi z_o}{c}\vec{e}_y\vec{e}_y\\ & +\left[k_0^2-\left(\frac{t\pi}{c}\right)^2\right]\sin\frac{r\pi x}{a}\sin\frac{r\pi x_o}{a}\sin\frac{s\pi y}{b}\sin\frac{s\pi y_o}{b}\cos\frac{t\pi z}{c}\cos\frac{t\pi z_o}{c}\vec{e}_z\vec{e}_z\\ & -\frac{rs\pi^2}{ab}\cos\frac{r\pi x}{a}\sin\frac{r\pi x_o}{a}\sin\frac{s\pi y}{b}\cos\frac{s\pi y_o}{b}\sin\frac{t\pi z}{c}\sin\frac{t\pi z_o}{c}\vec{e}_x\vec{e}_y\\ & -\frac{rs\pi^2}{ab}\sin\frac{r\pi x}{a}\cos\frac{r\pi x_o}{a}\cos\frac{s\pi y}{b}\sin\frac{s\pi y_o}{b}\sin\frac{t\pi z}{c}\sin\frac{t\pi z_o}{c}\vec{e}_y\vec{e}_x\\ & -\frac{st\pi^2}{bc}\sin\frac{r\pi x}{a}\sin\frac{r\pi x_o}{a}\cos\frac{s\pi y}{b}\sin\frac{s\pi y_o}{b}\sin\frac{t\pi z}{c}\cos\frac{t\pi z_o}{c}\vec{e}_y\vec{e}_z\\ & -\frac{st\pi^2}{bc}\sin\frac{r\pi x}{a}\sin\frac{r\pi x_o}{a}\sin\frac{s\pi y}{b}\cos\frac{s\pi y_o}{b}\cos\frac{t\pi z}{c}\sin\frac{t\pi z_o}{c}\vec{e}_z\vec{e}_y\\ & -\frac{rt\pi^2}{ac}\sin\frac{r\pi x}{a}\cos\frac{r\pi x_o}{a}\sin\frac{s\pi y}{b}\sin\frac{s\pi y_o}{b}\cos\frac{t\pi z}{c}\sin\frac{t\pi z_o}{c}\vec{e}_z\vec{e}_x\\ & \left.-\frac{rt\pi^2}{ac}\cos\frac{r\pi x}{a}\sin\frac{r\pi x_o}{a}\sin\frac{s\pi y}{b}\sin\frac{s\pi y_o}{b}\sin\frac{t\pi z}{c}\cos\frac{t\pi z_o}{c}\vec{e}_x\vec{e}_z\right]\end{aligned} \tag{3.10}$$

Note that the first three components ($\vec{e}_x\vec{e}_x, \vec{e}_y\vec{e}_y, \vec{e}_z\vec{e}_z$) of the Green's dyadic have the same symmetry properties. This fact will be used by the implementation of these functions in computer software. The last six components of the Green's dyadic have also equal symmetry properties. The second magnetic Green's function can be calculated by means of the eigenvectors $\vec{E}_{rst}$ and $\vec{H}_{rst}$.

The final result is given by

$$\begin{aligned}
\bar{\bar{G}}_m^2(\vec{r},\vec{r}_o) \;=\; & \sum_{r=0}^{\infty}\sum_{s=0}^{\infty}\sum_{t=0}^{\infty}\frac{\epsilon_{or}\epsilon_{os}\epsilon_{ot}}{abc\left(k_{rst}^2-k_0^2\right)} \\
& \left[\frac{t\pi}{c}\cos\frac{r\pi x}{a}\cos\frac{r\pi x_o}{a}\sin\frac{s\pi y}{b}\sin\frac{s\pi y_o}{b}\sin\frac{t\pi z}{c}\cos\frac{t\pi z_o}{c}\vec{e}_x\vec{e}_y\right. \\
& -\frac{t\pi}{c}\sin\frac{r\pi x}{a}\sin\frac{r\pi x_o}{a}\cos\frac{s\pi y}{b}\cos\frac{s\pi y_o}{b}\sin\frac{t\pi z}{c}\cos\frac{t\pi z_o}{c}\vec{e}_y\vec{e}_x \\
& \frac{r\pi}{a}\sin\frac{r\pi x}{a}\cos\frac{r\pi x_o}{a}\cos\frac{s\pi y}{b}\cos\frac{s\pi y_o}{b}\sin\frac{t\pi z}{c}\sin\frac{t\pi z_o}{c}\vec{e}_y\vec{e}_z \\
& -\frac{r\pi}{a}\sin\frac{r\pi x}{a}\cos\frac{r\pi x_o}{a}\sin\frac{s\pi y}{b}\sin\frac{s\pi y_o}{b}\cos\frac{t\pi z}{c}\cos\frac{t\pi z_o}{c}\vec{e}_z\vec{e}_y \\
& \frac{s\pi}{b}\sin\frac{r\pi x}{a}\sin\frac{r\pi x_o}{a}\sin\frac{s\pi y}{b}\cos\frac{s\pi y_o}{b}\cos\frac{t\pi z}{c}\cos\frac{t\pi z_o}{c}\vec{e}_z\vec{e}_x \\
& \left.-\frac{s\pi}{b}\cos\frac{r\pi x}{a}\cos\frac{r\pi x_o}{a}\sin\frac{s\pi y}{b}\cos\frac{s\pi y_o}{b}\sin\frac{t\pi z}{c}\sin\frac{t\pi z_o}{c}\vec{e}_x\vec{e}_z\right]
\end{aligned} \tag{3.11}$$

Note that the $\vec{e}_x\vec{e}_x$, $\vec{e}_y\vec{e}_y$ and $\vec{e}_z\vec{e}_z$ components of $\bar{\bar{G}}_m^2$ equal zero. With the above formulae the electric field due to an elementary electric and an elementary magnetic source inside a rectangular box cavity can be calculated. The electric field caused by an arbitrary source is given by equation (2.27):

$$\vec{E}(\vec{r}) = -j\omega\mu_0\int\int\int_{V_o}\bar{\bar{G}}_e^1(\vec{r},\vec{r}_o).\vec{J}_e(\vec{r}_o)dV_o - \int\int\int_{V_o}\bar{\bar{G}}_m^2(\vec{r},\vec{r}_o).\vec{J}_m(\vec{r}_o)dV_o. \tag{3.12}$$

When the volume source distributions $\vec{J}_e$ and $\vec{J}_m$ are known, the electric field can be calculated using (3.10), (3.11) and the above described relationship.

Now we will develop the three dimensional Green's functions for the magnetic field inside the cavity. Using the analysis described in chapter two, we know that the Green's functions used for the expansion of the magnetic field are given by

$$\begin{aligned}
\bar{\bar{G}}_m^1 &= \sum_{r=0}^{\infty}\sum_{s=0}^{\infty}\sum_{t=0}^{\infty}\frac{\vec{H}_{rst}(\vec{r})\vec{H}_{rst}(\vec{r}_o)}{k_{rst}^2-k_0^2} - \frac{1}{k_0^2}\sum_{r=0}^{\infty}\sum_{s=0}^{\infty}\sum_{t=0}^{\infty}\vec{K}_{rst}(\vec{r})\vec{K}_{rst}(\vec{r}_o), \\
\bar{\bar{G}}_e^2 &= \sum_{r=0}^{\infty}\sum_{s=0}^{\infty}\sum_{t=0}^{\infty}\frac{k_{rst}\vec{H}_{rst}(\vec{r})\vec{E}_{rst}(\vec{r}_o)}{k_{rst}^2-k_0^2}.
\end{aligned} \tag{3.13}$$

The magnetic field can be calculated in a similar way.

The first magnetic Green's dyadic is given by

$$\begin{aligned}
\bar{\bar{G}}_m^1(\vec{r},\vec{r}_o) \;=\; & \sum_{r=0}^{\infty}\sum_{s=0}^{\infty}\sum_{t=0}^{\infty}\frac{\epsilon_{or}\epsilon_{os}\epsilon_{ot}}{abc\left(k_{rst}^2-k_0^2\right)k_0^2} \\
& \left[\left[k_0^2-\left(\frac{r\pi}{a}\right)^2\right]\sin\frac{r\pi x}{a}\sin\frac{r\pi x_o}{a}\cos\frac{s\pi y}{b}\cos\frac{s\pi y_o}{b}\cos\frac{t\pi z}{c}\cos\frac{t\pi z_o}{c}\vec{e}_x\vec{e}_x\right. \\
& +\left[k_0^2-\left(\frac{s\pi}{b}\right)^2\right]\cos\frac{r\pi x}{a}\cos\frac{r\pi x_o}{a}\sin\frac{s\pi y}{b}\sin\frac{s\pi y_o}{b}\cos\frac{t\pi z}{c}\cos\frac{t\pi z_o}{c}\vec{e}_y\vec{e}_y \\
& +\left[k_0^2-\left(\frac{t\pi}{c}\right)^2\right]\cos\frac{r\pi x}{a}\cos\frac{r\pi x_o}{a}\cos\frac{s\pi y}{b}\cos\frac{s\pi y_o}{b}\sin\frac{t\pi z}{c}\sin\frac{t\pi z_o}{c}\vec{e}_z\vec{e}_z \\
& -\frac{rs\pi^2}{ab}\sin\frac{r\pi x}{a}\cos\frac{r\pi x_o}{a}\cos\frac{s\pi y}{b}\sin\frac{s\pi y_o}{b}\cos\frac{t\pi z}{c}\cos\frac{t\pi z_o}{c}\vec{e}_x\vec{e}_y \\
& -\frac{rs\pi^2}{ab}\cos\frac{r\pi x}{a}\sin\frac{r\pi x_o}{a}\sin\frac{s\pi y}{b}\cos\frac{s\pi y_o}{b}\cos\frac{t\pi z}{c}\cos\frac{t\pi z_o}{c}\vec{e}_y\vec{e}_x \\
& -\frac{st\pi^2}{bc}\cos\frac{r\pi x}{a}\cos\frac{r\pi x_o}{a}\sin\frac{s\pi y}{b}\cos\frac{s\pi y_o}{b}\cos\frac{t\pi z}{c}\sin\frac{t\pi z_o}{c}\vec{e}_y\vec{e}_z \\
& -\frac{st\pi^2}{bc}\cos\frac{r\pi x}{a}\cos\frac{r\pi x_o}{a}\cos\frac{s\pi y}{b}\sin\frac{s\pi y_o}{b}\sin\frac{t\pi z}{c}\cos\frac{t\pi z_o}{c}\vec{e}_z\vec{e}_y \\
& -\frac{rt\pi^2}{ac}\cos\frac{r\pi x}{a}\sin\frac{r\pi x_o}{a}\cos\frac{s\pi y}{b}\cos\frac{s\pi y_o}{b}\sin\frac{t\pi z}{c}\cos\frac{t\pi z_o}{c}\vec{e}_z\vec{e}_x \\
& \left.-\frac{rt\pi^2}{ac}\sin\frac{r\pi x}{a}\cos\frac{r\pi x_o}{a}\cos\frac{s\pi y}{b}\cos\frac{s\pi y_o}{b}\cos\frac{t\pi z}{c}\sin\frac{t\pi z_o}{c}\vec{e}_x\vec{e}_z\right].
\end{aligned} \tag{3.14}$$

The second electric Green's function is given by

$$\begin{aligned}
\bar{\bar{G}}_e^2(\vec{r},\vec{r}_o) \;=\; & \sum_{r=0}^{\infty}\sum_{s=0}^{\infty}\sum_{t=0}^{\infty}\frac{\epsilon_{or}\epsilon_{os}\epsilon_{ot}}{abc\left(k_{rst}^2-k_0^2\right)} \\
& \left[-\frac{t\pi}{c}\sin\frac{r\pi x}{a}\sin\frac{r\pi x_o}{a}\cos\frac{s\pi y}{b}\cos\frac{s\pi y_o}{b}\cos\frac{t\pi z}{c}\sin\frac{t\pi z_o}{c}\vec{e}_x\vec{e}_y\right. \\
& \frac{t\pi}{c}\cos\frac{r\pi x}{a}\cos\frac{r\pi x_o}{a}\sin\frac{s\pi y}{b}\sin\frac{s\pi y_o}{b}\cos\frac{t\pi z}{c}\sin\frac{t\pi z_o}{c}\vec{e}_y\vec{e}_x \\
& -\frac{r\pi}{a}\cos\frac{r\pi x}{a}\sin\frac{r\pi x_o}{a}\sin\frac{s\pi y}{b}\sin\frac{s\pi y_o}{b}\cos\frac{t\pi z}{c}\sin\frac{t\pi z_o}{c}\vec{e}_y\vec{e}_z \\
& \frac{r\pi}{a}\cos\frac{r\pi x}{a}\sin\frac{r\pi x_o}{a}\cos\frac{s\pi y}{b}\cos\frac{s\pi y_o}{b}\sin\frac{t\pi z}{c}\sin\frac{t\pi z_o}{c}\vec{e}_z\vec{e}_y \\
& -\frac{s\pi}{b}\cos\frac{r\pi x}{a}\cos\frac{r\pi x_o}{a}\cos\frac{s\pi y}{b}\sin\frac{s\pi y_o}{b}\sin\frac{t\pi z}{c}\sin\frac{t\pi z_o}{c}\vec{e}_z\vec{e}_x \\
& \left.\frac{s\pi}{b}\sin\frac{r\pi x}{a}\sin\frac{r\pi x_o}{a}\cos\frac{s\pi y}{b}\sin\frac{s\pi y_o}{b}\cos\frac{t\pi z}{c}\cos\frac{t\pi z_o}{c}\vec{e}_x\vec{e}_z\right].
\end{aligned} \tag{3.15}$$

The magnetic field excited by an arbitrary source is given by (2.28)

$$\vec{H}(\vec{r}) = -j\omega\epsilon_0\int\int\int_{V_o}\bar{\bar{G}}_m^1(\vec{r},\vec{r}_o).\vec{J}_m(\vec{r}_o)dV_o + \int\int\int_{V_o}\bar{\bar{G}}_e^2(\vec{r},\vec{r}_o).\vec{J}_e(\vec{r}_o)dV_o. \tag{3.16}$$

3.3 Double series representation of the Green's functions

The nine components of the Green's dyadic are now calculated using a triple series expansion. In order to reduce the computational effort, the Green's functions can be reduced to double series.

As mentioned in section 3.2, the longitudinal components of the Green's dyadic ($\vec{e}_x\vec{e}_x, \vec{e}_y\vec{e}_y, \vec{e}_z\vec{e}_z$) have the same symmetry properties. The G^{l}_{exx}-component is chosen in this section to illustrate the reduction of one series of a longitudinal component. Also the transverse components of the Green's dyadic have equal symmetry properties. The G^{l}_{eyx}-component is chosen in this section to illustrate the calculation of the closed form of a transverse component.

3.3.1 Elimination of one series of G^{l}_{exx}

Using (3.10), the longitudinal Green's function G^{l}_{exx} can be written as

$$\begin{aligned} G^{\mathrm{l}}_{exx} &= \sum_{r=0}^{\infty}\sum_{s=0}^{\infty} \frac{4\epsilon_{or}}{abck_0^2}\left[k_0^2 - \left(\frac{r\pi}{a}\right)^2\right]\cos\frac{r\pi x}{a}\cos\frac{r\pi x_o}{a}\sin\frac{s\pi y}{b}\sin\frac{s\pi y_o}{b} \\ &\quad \sum_{t=0}^{\infty}\frac{\sin\frac{t\pi z}{c}\sin\frac{t\pi z_o}{c}}{k_{rst}^2 - k_0^2}. \end{aligned} \tag{3.17}$$

The last series will be calculated in closed form. We shall consider two regions.

1. $\left(\frac{rc}{a}\right)^2 + \left(\frac{sc}{b}\right)^2 - \left(\frac{k_0 c}{\pi}\right)^2 \geq 0$

G^{l}_{exx} is written in the following form

$$G^{\mathrm{l}}_{exx} = \delta\frac{c^2}{\pi^2}\sum_{t=1}^{\infty}\frac{\sin\frac{t\pi z}{c}\sin\frac{t\pi z_o}{c}}{t^2+\alpha_1^2}, \tag{3.18}$$

where the variables δ and α_1 are given by

$$\delta = \sum_{r=0}^{\infty}\sum_{s=0}^{\infty}\frac{4\epsilon_{or}}{abck_0^2}\left(k_0^2 - \left(\frac{r\pi}{a}\right)^2\right)\cos\frac{r\pi x}{a}\cos\frac{r\pi x_o}{a}\sin\frac{s\pi y}{b}\sin\frac{s\pi y_o}{b}, \tag{3.19}$$

$$\alpha_1 = \sqrt{\left(\frac{rc}{a}\right)^2 + \left(\frac{sc}{b}\right)^2 - \left(\frac{k_0 c}{\pi}\right)^2}. \tag{3.20}$$

The above mentioned series can be written as

$$G^{\mathrm{l}}_{exx} = \frac{\delta}{2}\left(\frac{c}{\pi}\right)^2\left[\sum_{t=0}^{\infty}\frac{\cos t(z-z_o)\pi/c}{t^2+\alpha_1^2} - \sum_{t=0}^{\infty}\frac{\cos t(z+z_o)\pi/c}{t^2+\alpha_1^2}\right]. \tag{3.21}$$

The closed form expressions of these series are well known in literature. Using a known summation result [15], the following relationship can be used

$$\sum_{k=1}^{\infty}\frac{\cos kx}{k^2+\alpha_1^2} = \frac{\pi}{2\alpha_1}\frac{\cosh\alpha_1(\pi-x)}{\sinh\alpha_1\pi} - \frac{1}{2\alpha_1^2} \qquad 0\leq x\leq 2\pi. \tag{3.22}$$

2. $\left(\frac{rc}{a}\right)^2 + \left(\frac{sc}{b}\right)^2 - \left(\frac{k_0 c}{\pi}\right)^2 < 0$

In this region G^1_{exx} is written as

$$G^1_{exx} = \delta \frac{c^2}{\pi^2} \sum_{t=1}^{\infty} \frac{\sin \frac{t\pi z}{c} \sin \frac{t\pi z_o}{c}}{t^2 - \alpha_2^2}, \tag{3.23}$$

where

$$\alpha_2 = \sqrt{\left(\frac{k_0 c}{\pi}\right)^2 - \left(\frac{rc}{a}\right)^2 - \left(\frac{sc}{b}\right)^2}. \tag{3.24}$$

Using [15], the following relationship can be used

$$\sum_{k=1}^{\infty} \frac{\cos kx}{k^2 - \alpha_2^2} = \frac{1}{2\alpha_2^2} - \frac{\pi}{2\alpha_2} \frac{\cos \alpha_2(\pi - x)}{\sin \alpha_2 \pi} \qquad 0 \le x \le 2\pi. \tag{3.25}$$

The expression of G^1_{exx} consists of the term $(z - z_o)\frac{\pi}{c}$, which value is located in the interval $[-\pi, \pi]$. Therefore we shall distinguish two regions: $z \ge z_o$ and $z < z_o$

1. $\left(\frac{rc}{a}\right)^2 + \left(\frac{sc}{b}\right)^2 - \left(\frac{k_0 c}{\pi}\right)^2 \ge 0$

- $z \ge z_o$. The final expression of the Green's function G^1_{exx} can be expressed as

$$\begin{aligned} G^1_{exx} = & \frac{2c}{abk_0^2\pi} \sum_{r=0}^{\infty} \sum_{s=1}^{\infty} \frac{\epsilon_{or}(k_0^2 - (\frac{r\pi}{a})^2)}{\alpha_1 \sinh \alpha_1 \pi} \\ & \cos \frac{r\pi x}{a} \cos \frac{r\pi x_o}{a} \sin \frac{s\pi y}{b} \sin \frac{s\pi y_o}{b} \sinh \alpha_1 (\pi - \frac{\pi}{c} z) \sinh \alpha_1 \frac{\pi}{c} z_o \end{aligned} \tag{3.26}$$

- $z < z_o$. G^1_{exx} can be written as follows

$$\begin{aligned} G^1_{exx} = & \frac{2c}{abk_0^2\pi} \sum_{r=0}^{\infty} \sum_{s=1}^{\infty} \frac{\epsilon_{or}(k_0^2 - (\frac{r\pi}{a})^2)}{\alpha_1 \sinh \alpha_1 \pi} \\ & \cos \frac{r\pi x}{a} \cos \frac{r\pi x_o}{a} \sin \frac{s\pi y}{b} \sin \frac{s\pi y_o}{b} \sinh \alpha_1 (\pi - \frac{\pi}{c} z_o) \sinh \alpha_1 \frac{\pi}{c} z. \end{aligned} \tag{3.27}$$

2. $\left(\frac{rc}{a}\right)^2 + \left(\frac{sc}{b}\right)^2 - \left(\frac{k_0 c}{\pi}\right)^2 < 0$

- $z \ge z_o$.

$$\begin{aligned} G^1_{exx} = & \frac{2c}{abk_0^2\pi} \sum_{r=0}^{\infty} \sum_{s=1}^{\infty} \frac{\epsilon_{or}(k_0^2 - (\frac{r\pi}{a})^2)}{\alpha_2 \sin \alpha_2 \pi} \\ & \cos \frac{r\pi x}{a} \cos \frac{r\pi x_o}{a} \sin \frac{s\pi y}{b} \sin \frac{s\pi y_o}{b} \sin \alpha_2 (\pi - \frac{\pi}{c} z) \sin \alpha_2 \frac{\pi}{c} z_o. \end{aligned} \tag{3.28}$$

- $z < z_o$.

$$G^{\mathrm{I}}_{exx} = \frac{2c}{abk_0^2\pi}\sum_{r=0}^{\infty}\sum_{s=1}^{\infty}\frac{\epsilon_{or}(k_0^2-(\frac{r\pi}{a})^2)}{\alpha_2\sin\alpha_2\pi} \cos\frac{r\pi x}{a}\cos\frac{r\pi x_o}{a}\sin\frac{s\pi y}{b}\sin\frac{s\pi y_o}{b}\sin\alpha_2(\pi-\frac{\pi}{c}z_o)\sin\alpha_2\frac{\pi}{c}z. \tag{3.29}$$

The series used for the calculation of G^{I}_{eyy} and G^{I}_{ezz} have similar forms, therefore the corresponding double series can be calculated in a similar way. Note that the choice of reducing the series over the variable t is arbitrary. Calculating one of the two other series in closed form yields different representations for the Green's functions. These representations might have different convergence properties, this will be shown later on in chapter four.

3.3.2 Elimination of one series of G^{I}_{eyx}

The Green's function G^{I}_{eyx} can be written as

$$G^{\mathrm{I}}_{eyx} = -\sum_{r=0}^{\infty}\sum_{s=0}^{\infty}\frac{8rs\pi^2}{a^2b^2ck_0^2}\sin\frac{r\pi x}{a}\cos\frac{r\pi x_o}{a}\cos\frac{s\pi y}{b}\sin\frac{s\pi y_o}{b} \sum_{t=0}^{\infty}\frac{\sin\frac{t\pi z}{c}\sin\frac{t\pi z_o}{c}}{k_{rst}^2-k_0^2}. \tag{3.30}$$

The last series will be expressed in closed form. There are again two situations:

1. $(\frac{rc}{a})^2+(\frac{sc}{b})^2-\left(\frac{k_0c}{\pi}\right)^2\geq 0$

- $z \geq z_o$. In this situation, the final expression of the Green's function G^{I}_{eyx} can be expressed as

$$G^{\mathrm{I}}_{eyx} = \frac{-4c\pi}{a^2b^2k_0^2}\sum_{r=1}^{\infty}\sum_{s=1}^{\infty}\frac{rs}{\alpha_1\sinh\alpha_1\pi} \sin\frac{r\pi x}{a}\cos\frac{r\pi x_o}{a}\cos\frac{s\pi y}{b}\sin\frac{s\pi y_o}{b}\sinh\alpha_1(\pi-\frac{\pi}{c}z)\sinh\alpha_1\frac{\pi}{c}z_o. \tag{3.31}$$

- $z < z_o$. G^{I}_{eyx} can be written as follows

$$G^{\mathrm{I}}_{eyx} = \frac{-4c\pi}{a^2b^2k_0^2}\sum_{r=1}^{\infty}\sum_{s=1}^{\infty}\frac{rs}{\alpha_1\sinh\alpha_1\pi} \sin\frac{r\pi x}{a}\cos\frac{r\pi x_o}{a}\cos\frac{s\pi y}{b}\sin\frac{s\pi y_o}{b}\sinh\alpha_1(\pi-\frac{\pi}{c}z_o)\sinh\alpha_1\frac{\pi}{c}z. \tag{3.32}$$

2. $(\frac{rc}{a})^2+(\frac{sc}{b})^2-\left(\frac{k_0c}{\pi}\right)^2<0$

- $z \geq z_o$. In this situation, the final expression of the Green's function G^{I}_{eyx} can be expressed as

$$G^{\mathrm{I}}_{eyx} = \frac{-4c\pi}{a^2b^2k_0^2}\sum_{r=1}^{\infty}\sum_{s=1}^{\infty}\frac{rs}{\alpha_2\sin\alpha_2\pi} \sin\frac{r\pi x}{a}\cos\frac{r\pi x_o}{a}\cos\frac{s\pi y}{b}\sin\frac{s\pi y_o}{b}\sin\alpha_2(\pi-\frac{\pi}{c}z)\sin\alpha_2\frac{\pi}{c}z_o. \tag{3.33}$$

- $z < z_o$. G^1_{eyx} can be written as follows

$$G^1_{eyx} = \frac{-4c\pi}{a^2b^2k_0^2}\sum_{r=1}^{\infty}\sum_{s=1}^{\infty}\frac{rs}{\alpha_2 \sin\alpha_2\pi} \sin\frac{r\pi x}{a}\cos\frac{r\pi x_o}{a}\cos\frac{s\pi y}{b}\sin\frac{s\pi y_o}{b}\sin\alpha_2(\pi-\frac{\pi}{c}z_o)\sin\alpha_2\frac{\pi}{c}z. \tag{3.34}$$

Various forms of the Green's function G^1_{eyx} can be obtained by choosing which series will be calculated in closed form. In this section another representation of G^1_{eyx} will be determined. The Green's function is written in the following form

$$G^1_{eyx} = -\sum_{r=0}^{\infty}\sum_{t=0}^{\infty}\frac{8r\pi}{a^2bck_0^2}\sin\frac{r\pi x}{a}\cos\frac{r\pi x_o}{a}\sin\frac{t\pi z}{c}\sin\frac{t\pi z_o}{c} \sum_{s=0}^{\infty}\frac{s\pi}{b}\frac{\cos\frac{s\pi y}{b}\sin\frac{s\pi y_o}{b}}{k_{rst}^2-k_0^2}. \tag{3.35}$$

The closed form expression of the last series is also known in literature. Using [15], the following equations are valid

$$\sum_{k=1}^{\infty}\frac{k\sin kx}{k^2+\beta_1^2} = \frac{\pi}{2}\frac{\sinh\beta_1(\pi-x)}{\sinh\beta_1\pi} \qquad 0<x<2\pi, \tag{3.36}$$

$$\sum_{k=1}^{\infty}\frac{k\sin kx}{k^2-\beta_2^2} = \frac{\pi}{2}\frac{\sin\beta_2(\pi-x)}{\sin\beta_2\pi} \qquad 0<x<2\pi. \tag{3.37}$$

where

$$\beta_1 = \sqrt{\left(\frac{rb}{a}\right)^2+\left(\frac{tb}{c}\right)^2-\left(\frac{k_0b}{\pi}\right)^2}, \tag{3.38}$$

$$\beta_2 = \sqrt{\left(\frac{k_0b}{\pi}\right)^2-\left(\frac{rb}{a}\right)^2-\left(\frac{tb}{c}\right)^2}. \tag{3.39}$$

The solution of G^1_{eyx} is divided in two regions

1. $\left(\frac{rb}{a}\right)^2+\left(\frac{tb}{c}\right)^2-\left(\frac{k_0b}{\pi}\right)^2 \geq 0$

- $y \geq y_o$. The expression of the Green's function G^1_{eyx} in this area can be expressed as

$$G^1_{eyx} = \frac{4\pi}{a^2ck_0^2}\sum_{r=0}^{\infty}\sum_{t=0}^{\infty}\frac{r}{\sinh\beta_1\pi} \sin\frac{r\pi x}{a}\cos\frac{r\pi x_o}{a}\sin\frac{t\pi z}{c}\sin\frac{t\pi z_o}{c}\cosh\beta_1(\pi-\frac{\pi}{b}y)\sinh\beta_1\frac{\pi}{b}y_o. \tag{3.40}$$

- $y < y_o$. G^1_{eyx} can be written as follows

$$G^1_{eyx} = \frac{-4\pi}{a^2ck_0^2}\sum_{r=0}^{\infty}\sum_{t=0}^{\infty}\frac{r}{\sinh\beta_1\pi} \sin\frac{r\pi x}{a}\cos\frac{r\pi x_o}{a}\sin\frac{t\pi z}{c}\sin\frac{t\pi z_o}{c}\sinh\beta_1(\pi-\frac{\pi}{b}y_o)\cosh\beta_1\frac{\pi}{b}y. \tag{3.41}$$

2. $\left(\frac{rb}{a}\right)^2 + \left(\frac{tb}{c}\right)^2 - \left(\frac{k_0 b}{\pi}\right)^2 < 0$

- $y \geq y_o$.

$$G^{\mathrm{I}}_{eyx} = \frac{4\pi}{a^2 c k_0^2} \sum_{r=0}^{\infty} \sum_{t=0}^{\infty} \frac{r}{\sin \beta_2 \pi} \sin \frac{r\pi x}{a} \cos \frac{r\pi x_o}{a} \sin \frac{t\pi z}{c} \sin \frac{t\pi z_o}{c} \cos \beta_2 (\pi - \frac{\pi}{b} y) \sin \beta_2 \frac{\pi}{b} y_o. \tag{3.42}$$

- $y < y_o$.

$$G^{\mathrm{I}}_{eyx} = \frac{-4\pi}{a^2 c k_0^2} \sum_{r=0}^{\infty} \sum_{t=0}^{\infty} \frac{r}{\sin \beta_2 \pi} \sin \frac{r\pi x}{a} \cos \frac{r\pi x_o}{a} \sin \frac{t\pi z}{c} \sin \frac{t\pi z_o}{c} \sin \beta_2 (\pi - \frac{\pi}{b} y_o) \cos \beta_2 \frac{\pi}{b} y. \tag{3.43}$$

The calculation of the double series of the other transverse components ($G^{\mathrm{I}}_{exy}, G^{\mathrm{I}}_{ezx}, G^{\mathrm{I}}_{exz}$) and ($G^{\mathrm{I}}_{ezy}, G^{\mathrm{I}}_{eyz}$) can be done in a similar way. By expressing different series in closed form, various representations of the Green's functions are obtained.

3.4 Conclusions

In this chapter descriptions of the electromagnetic fields are obtained inside a rectangular cavity. The source inside the cavity, which excites the electromagnetic fields, is an arbitrary polarised magnetic or electric dipole. Four Green's dyadics are needed in order to calculate the electromagnetic fields. The components of these various dyadics can be expressed as triple series expansions using eigenvectors. In the last section of this chapter, one series is calculated in closed form, so the Green's functions are described by double series. Because we can choose which series will be evaluated in closed form, various representations of the Green's functions are obtained. It will be shown in chapter four that these various forms of the Green's functions have different convergence behaviours at some regions inside the cavity. This knowledge will be used when implementing the numerical algorithms.

Chapter 4

Results

4.1 Introduction

Our main interest concerns the intensities and the polarisations of the electromagnetic fields inside the cavity. Using the analytical results derived in earlier chapters, we are now able to calculate the six field components caused by an elementary source. Another concern will be the numerical problems at the singularity points of the various Green's functions. Therefore much attention will be given to the evaluation of the convergence properties of the Green's functions in this chapter.

Some examples of field structures inside a particular cavity are presented in section 4.2. Due to the singularity of the field, the convergence of the series in the neighbourhood of the source is very slow. Furthermore it will be shown that the convergence might be slow at some other regions inside the cavity, depending on which summation is calculated in closed form. In section 4.3, convergence properties of the double series are compared with each other. The convergence behaviour of the series are visualized by calculating the partial sums of the series. Finally, the electromagnetic fields inside a cavity will be compared to the free space fields in section 4.4.

4.2 Electromagnetic fields inside a rectangular cavity

In this section the electromagnetic fields inside a cavity will be visualized. The model outlined in the previous chapter is implemented in a FORTRAN code. With the help of this program, the electromagnetic fields caused by an electric or magnetic point source can be calculated. The wavelengths of the electromagnetic fields are much smaller than the dimensions of the cavity. This means that the amplitudes of the electromagnetic fields change very rapidly inside the cavity. In order to present a clear picture, the electromagnetic fields will not be calculated inside the entire cavity. The plane in which we will calculate the fields is called observation plane.

The geometry of the cavity is given by figure 3.1. The dimensions (a, b, c) of the cavity are equal to (5.4 m, 3.7 m, 2.2 m). The wavelength of the monochromatic transmitted wave is 15 cm. The point source is located at the coordinates ($a/4, b/2, c/2$). The electric source is directed into the z-direction. Furthermore, the z-coordinate of the observation plane is equal to c/2, this means that the x- and y-polarised electric fields are zero in this plane.
Only the electric field in the shaded region of figure 4.1 will be calculated. The absolute value of the electric field into the z-direction is presented in figure 4.2.

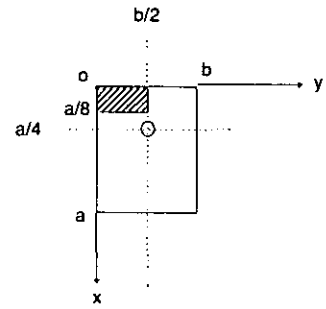

Figure 4.1: *Observation plane*

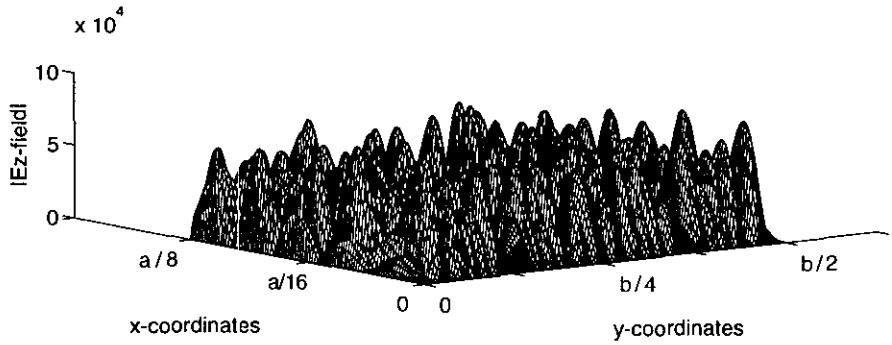

Figure 4.2: *Ez-field at the observation plane*

It is clear from figure 4.2 that the absolute value of the electric field changes rapidly. Because the walls of the cavity are perfectly conducting, there will be many standing waves inside the cavity.

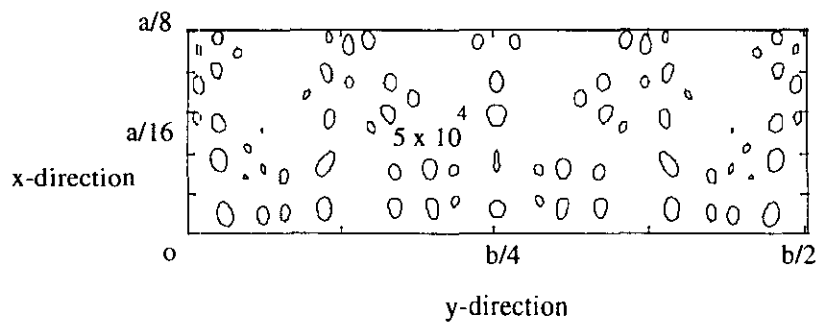

Figure 4.3: *Contour plot*

The maximum values of the electric field at the observation plane are presented in figure 4.3. The regions inside the closed contours have electric field components larger than 50000 V/m. The same calculations have been made for the magnetic fields at the observation plane. The magnetic field into the z-direction is zero inside the cavity. The magnetic field into the x-direction is given by figure 4.4. The y-polarised magnetic fields have similar forms as shown in figure 4.4, therefore they will not be presented here.

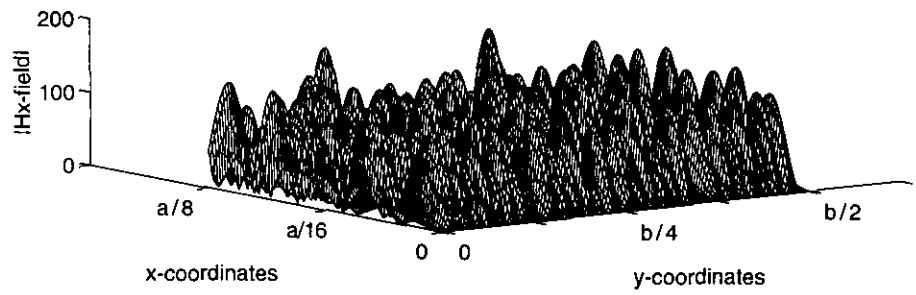

Figure 4.4: *Hx-field at the observation plane*

4.3 Convergence properties of various series representations

In chapter three, various representations of the Green's functions for a rectangular cavity have been analysed. In this section, some convergence properties of these Green's functions will be investigated. The series, representing the electromagnetic fields, have complex arguments. Unfortunately, it is not possible to evaluate the convergence properties of these series in a strict mathematical sense. However, the convergence properties will be evaluated by a numerical analysis. Only the dyadic $\bar{\bar{G}}_e$, which represents the electric field caused by an electric point source, will be evaluated. The other dyadics have similar forms, so the analysis presented in this section can be used for the calculation of the other dyadics as well. The electromagnetic field in the cavity will be calculated using double series and the convergence properties of these double series will be analyzed by determining the partial sums. The partial sums of a double series are given by

$$S_n = \sum_{r=0}^{n} \sum_{s=0}^{n} f(r,s) \tag{4.1}$$

The electromagnetic field at the observation plane is calculated twice. The first calculation has been made by taking the partial sum index equal to 60. The second calculation has been made by taking the sum index equal to 80. The differences between the two obtained results are calculated by

$$\beta = \frac{S_{80} - S_{60}}{S_{60}} \times 100\% \tag{4.2}$$

The observation plane for which the electromagnetic fields will be calculated is shown in figure 4.5. Due to the fact that the source is located in the observation plane, we are able to evaluate the convergence properties of the series at the singularities.

The dimensions of the cavity (a,b,c) are equal to (3.4 m, 3.7 m, 2.2 m). The electric source is directed into the z-direction. The frequency is 2 GHz.

First the electric field into the z-direction will be determined. Using the double series representation, the difference factor β at the observation plane is shown in figure 4.6.

The points between closed contours have a minimal β-factor of 5 percent. It is remarkable that the convergence is not only slow at the source coordinates but also around $x = a/4$. Remember that the

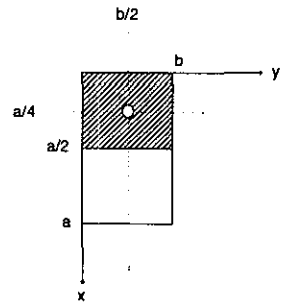

Figure 4.5: *Observation Plane*

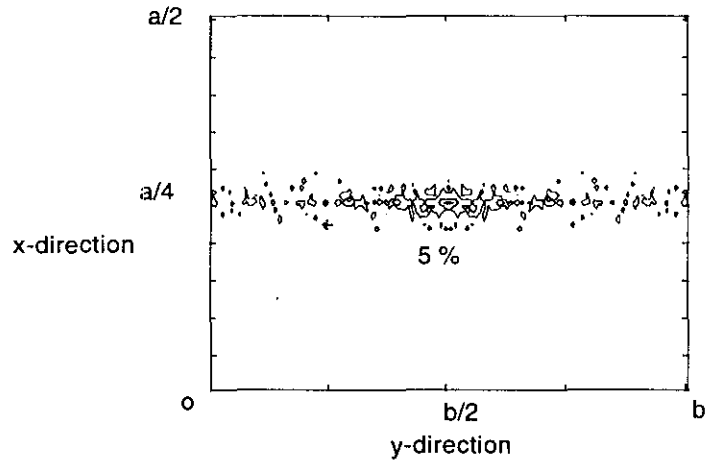

Figure 4.6: *Difference factor β at the observation plane*

Green's function G^{I}_{ezz} is given by the following equation

$$G^{\mathrm{I}}_{ezz} = \sum_{s=0}^{\infty}\sum_{t=0}^{\infty} \frac{\epsilon_{or}\epsilon_{os}\epsilon_{ot}}{abck_0^2}\left[k_0^2 - \left(\frac{t\pi}{c}\right)^2\right] \sin\frac{s\pi y}{b} \sin\frac{s\pi y_o}{b} \cos\frac{t\pi z}{c} \cos\frac{t\pi z_o}{c} \sum_{r=0}^{\infty} \frac{1}{k_{rst}^2 - k_0^2} \sin\frac{r\pi x}{a} \sin\frac{r\pi x_o}{a} \tag{4.3}$$

This equation, which consists of a triple series, can be transformed into a double series in three ways by choosing which series will be written in closed form. In the above figure, the fields are calculated by writing the last series in closed form. This series contains the field coordinates x and source coordinates x_o. From the above figure it is clear that the convergence will be slow when the coordinates x and x_o are close together. In this case, there will always be a region with slow convergence properties no matter which of the three series will be calculated in closed form.

We will change the z_o coordinate of the source into 0.21 m. The series containing the coordinates z and z_o will be calculated in closed form. At the observation plane, the coordinates z and z_o will never be close together. So it can be expected that the convergence of the Green's function G^{I}_{ezz} will be fast. For this case, the difference factor β is calculated. Using numerical calculations it has been verified that the factor β is less than 10^{-5} at the observation plane. In order to check the earlier stated assumptions, the difference factors of the fields into the x- and y-directions have also been calculated.

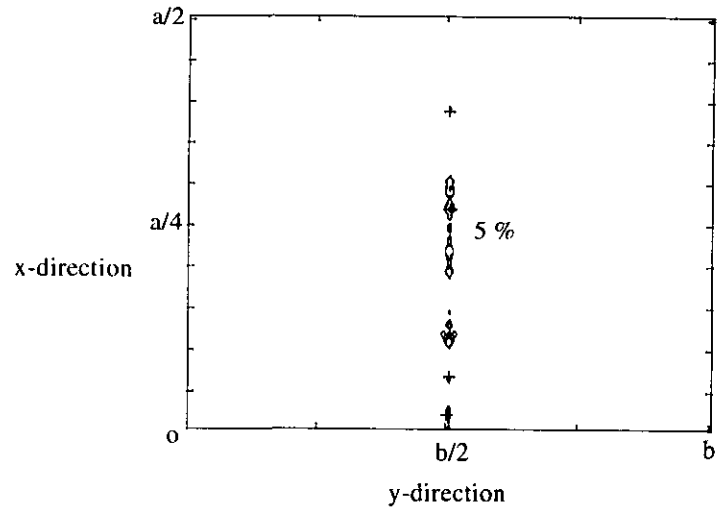

Figure 4.7: *Difference factor β of x-polarised electric field*

One series of the triple series describing the x-polarised electric field is also written in closed form. The fields are calculated by closing the series containing the coordinates y and y_o. Again, the double series is slowly convergent when the coordinates y and y_o are close together.

The convergence properties of the electric field into the y-direction is given by figure 4.8.

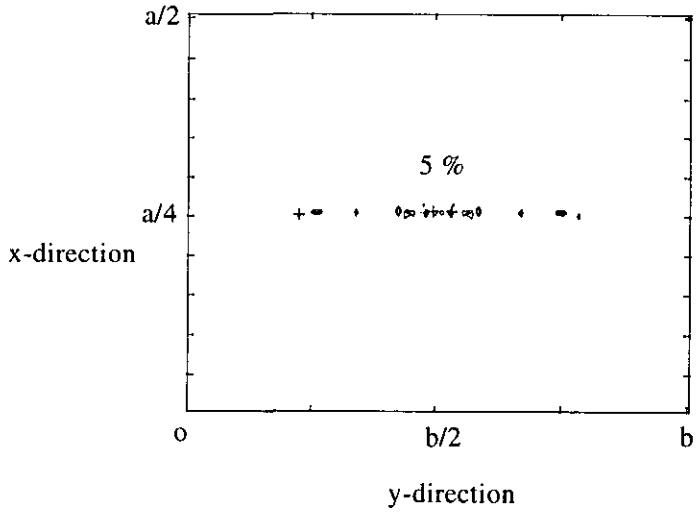

Figure 4.8: *Difference factor β of y-polarised electric field*

The electric fields into the y-direction have been calculated by closing the series containing the coordinates x and x_o. Again, the double series is slowly convergent when the observation and source coordinates x and x_o are close together.

4.4 Fields inside a cavity and in free space

The electromagnetic waves inside a cavity will be reflected when they approach the perfectly conducting walls. Therefore the electromagnetic fields at the field points consist not only the direct wave but

also some reflected waves. So the multipath components arrive at the receiver in various directions [16]. This is a typical situation in a multipath environment. In order to make an estimation of the influence of the multipath environment, we will compare the electromagnetic fields inside the cavity with the electromagnetic fields in free space.

The source will be a z-directed dipole. The geometry of the cavity is given by figure 2.1. Just like presented in section 4.2, the dimensions (a, b, c) of the cavity will be equal to (5.4 m, 3.7 m, 2.2 m). The wavelength of the electromagnetic field is 15 cm. The source is located at the source coordinates (a/4, b/2, c/2). The z-coordinate of the observation plane is equal to c/2 and this plane is presented by figure 4.1.

The fields in free space excited by an elementary source are calculated in appendix A. In section 4.2 it is stated that the x- and y-directed electric fields are zero at the observation plane due to the fact that the coordinates z and z_o are equal to $c/2$. According to appendix A, the x-directed and y-directed electric fields are also equal to zero in free space. So we will calculate the free space field $\vec{E}_{free\ space}$ only for the z-directed components. The free space electric field is shown in figure 4.9.

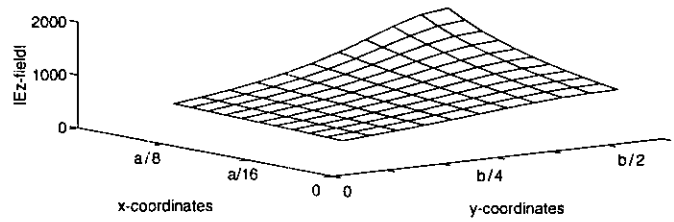

Figure 4.9: *Electric field in free space*

There are no standing waves in the free space environment. It is clear from figure 4.9 that the strengths of the fields in the free space environment differs to the fields in the multipath environment.

The x-directed magnetic field in free space is given by figure 4.10.

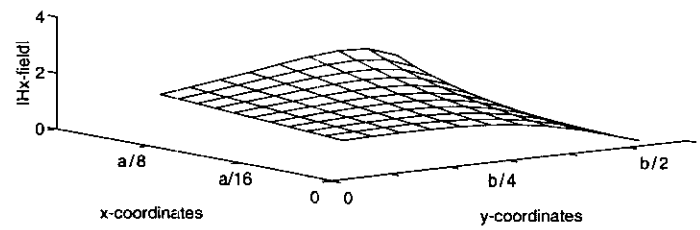

Figure 4.10: *Hx-field in free space*

4.5 Conclusions

The electromagnetic fields for a particular cavity have been visualized in section 4.2. Due to the fact that the wavelength is small compared to the dimensions of the cavity, there are many standing waves

inside the cavity. There are many spots inside the indoor environment where several components of the electric or magnetic field vanish. Inside these regions, it is to be expected that the noise level exceeds the signal strength, so the telecommunication link will be disturbed.

In section 4.3 some convergence properties of Green's functions are investigated. It has been shown that the fields are slowly convergent not only near the singularity, but also in some other regions inside the cavity, depending on which series will be calculated in closed form. Therefore much care must be taken by choosing which representation of the Green's function will be used for the determination of the electromagnetic fields.

The electromagnetic fields inside the cavity have been compared with the electromagnetic fields in free space in order to determine the influence of the multipath environment. In section 4.4 it has been shown that propagation inside the multipath environment (cavity) differs much to the free space electromagnetic fields.

Chapter 5

Singularity extraction

5.1 Introduction

In the previous chapter it has been shown that the Green's functions of a rectangular cavity are slowly convergent when the observation coordinates are close to the source coordinates. This can be a serious problem because Green's functions are used in numerical methods, which often require the computation of the Green's function inside the source region. Therefore the previous expressions for the Green's functions are not well suited for the computation of the electromagnetic field calculated by integral equations.
To overcome this problem the Green's functions will be split into three parts. The first Green's function has a singularity of the order $\frac{1}{R^3}$, where R is the distance between the observation coordinates and the source coordinates. This function contains the dominant singularity. The second Green's function consists of a weaker singularity, this function is singular like $\frac{1}{R}$. The third Green's function describes the resonances of the cavity. Unlike the original Green's functions, the third Green's function is finite at the source coordinates.

5.2 Decomposition of the Green's function

Several authors [17], [18] have considered the extraction of the dominant singularity ($\frac{1}{R^3}$) for various Green's functions. The resulting series converges better than the original series, but the convergence is still slow. This can be explained by noting that the series still contains a singularity like $\frac{1}{R}$.
Bressan and Conciauro [19] decomposes the Green's function for a closed region in three parts. The first dyadic represents the irrotational part of the original dyadic and diverges like $\frac{1}{R^3}$. The second dyadic and the third dyadic are solenoidal. The second dyadic diverges like $\frac{1}{R}$ and the third dyadic is finite at the source coordinates. So the Green's dyadic can be written as

$$\bar{\bar{G}}_e^{\,\mathrm{I}}(\vec{r},\vec{r}_o) = \bar{\bar{G}}_1(\vec{r},\vec{r}_o) + \bar{\bar{G}}_2(\vec{r},\vec{r}_o) + \bar{\bar{G}}_3(\vec{r},\vec{r}_o). \tag{5.1}$$

It has been shown in chapter two that four Green's dyadics are needed to calculate the electromagnetic field caused by an electric or magnetic point source. Because many components of these dyadics have equal forms, only the extraction of the singularity for the dyadic $\bar{\bar{G}}_e^{\,\mathrm{I}}$ will be considered in this chapter. It has been pointed out by several authors that the singularity of the function $\bar{\bar{G}}_e^{\,\mathrm{I}}$ is essentially the same as the one of the free space Green's function $\bar{\bar{G}}_o$. The dyadic $\bar{\bar{G}}_o$ is given by the following equation

$$\bar{\bar{G}}_o(\vec{r},\vec{r}_o) = \left(\bar{\bar{I}} + \frac{1}{k_0^2}\nabla\nabla\right)\frac{e^{-jk_0R}}{4\pi R}, \tag{5.2}$$

where $R = |\vec{r} - \vec{r}_o|$. The symbol $\bar{\bar{I}}$ represents the unit dyadic. The free space Green's function can be approximated by expanding the exponential of the function in a Taylor series. The following approximation is obtained

$$\bar{\bar{G}}_o \approx \frac{1}{k_0^2}\nabla\nabla\frac{1}{4\pi R} + \frac{1}{8\pi R}\left(\bar{\bar{I}} + \frac{(\vec{r}-\vec{r}_o)(\vec{r}-\vec{r}_o)}{R^2}\right). \tag{5.3}$$

In this expansion all terms finite at $R = 0$ are neglected. From this expansion it can be deduced that the dominant singularity is given by the term $\frac{1}{k_0^2}\nabla\nabla\frac{1}{4\pi R}$, which is irrotational. The weaker singularity is given by the solenoidal term $\frac{1}{8\pi R}\left[\bar{\bar{I}} + \frac{(\vec{r}-\vec{r}_o)(\vec{r}-\vec{r}_o)}{R^2}\right]$. As an example only the singularity extraction of the functions G^1_{exx} and G^1_{eyx} will be calculated. The singularities of the other components of the four Green's dyadics can be extracted in a similar manner. Therefore only the dyadic $\bar{\bar{G}}^1_e$ will be considered in the following analysis.

The first decomposition is given by the following equation

$$\bar{\bar{G}}^1_e(\vec{r},\vec{r}_o) = -\frac{1}{k_0^2}\nabla\nabla_o g(\vec{r},\vec{r}_o) + \bar{\bar{G}}_2(\vec{r},\vec{r}_o) + \bar{\bar{G}}_3(\vec{r},\vec{r}_o), \tag{5.4}$$

where ∇_o means differentiation with respect to the source coordinates. The function $g(\vec{r},\vec{r}_o)$ is a scalar Green's function. The three components g, $\bar{\bar{G}}_2$ and $\bar{\bar{G}}_3$ are related by the following relationships

$$\nabla^2 g(\vec{r},\vec{r}_o) = -\delta(\vec{r}-\vec{r}_o), \tag{5.5}$$

$$\nabla\times\nabla\times\bar{\bar{G}}_2(\vec{r},\vec{r}_o) = \bar{\bar{I}}\delta(\vec{r}-\vec{r}_o) - \nabla\nabla_o g(\vec{r},\vec{r}_o), \tag{5.6}$$

$$\nabla\times\nabla\times\bar{\bar{G}}_3(\vec{r},\vec{r}_o) - k_0^2\bar{\bar{G}}_3(\vec{r},\vec{r}_o) = k_0^2\bar{\bar{G}}_2(\vec{r},\vec{r}_o), \tag{5.7}$$

in the internal cavity volume V. The boundary conditions are given by

$$g = 0 \qquad \vec{n}\times\bar{\bar{G}}_2 = \bar{\bar{0}} \qquad \vec{n}\times\bar{\bar{G}}_3 = \bar{\bar{0}}. \tag{5.8}$$

Taking the curl of the curl of (5.4) and using (5.5), (5.6), (5.7) results in

$$\nabla\times\nabla\times\bar{\bar{G}}^1_e(\vec{r},\vec{r}_o) - k_0^2\bar{\bar{G}}^1_e(\vec{r},\vec{r}_o) = \bar{\bar{I}}\delta(\vec{r}-\vec{r}_o). \tag{5.9}$$

Notice that this result is the same as equation (2.22), which has been used for the definition of the Green's dyadic $\bar{\bar{G}}_e$. Using the above equations, the components $\bar{\bar{G}}_1$, $\bar{\bar{G}}_2$ and $\bar{\bar{G}}_3$ can be calculated.

Unfortunately this is a tedious process, therefore other relationships will be derived in the next sections in order to solve the three Green's dyadics. First we note that the weakly singular term of the Taylor expansion of the free space Green's function is k_0 - independent. The solenoidal dyadic $\bar{\bar{G}}_2$ is also k_0 -independent according to equation (5.6). Therefore the dyadic $\bar{\bar{G}}_2$ will be written as

$$\bar{\bar{G}}_2(\vec{r},\vec{r}_o) = \frac{1}{8\pi R}\left(\bar{\bar{I}} + \frac{(\vec{r}-\vec{r}_o)(\vec{r}-\vec{r}_o)}{R^2}\right) + \bar{\bar{G}}_{2o}(\vec{r},\vec{r}_o), \tag{5.10}$$

where $\bar{\bar{G}}_{2o}$ is a k_0 -independent dyadic and finite at the source coordinates. So the dyadic $\bar{\bar{G}}_2$ consists of a regular and a singular part. Using the analysis described in [19], the third Green's function $\bar{\bar{G}}_3(\vec{r},\vec{r}_o)$ will be expressed as

$$\bar{\bar{G}}_3(\vec{r},\vec{r}_o) = \sum_{r=0}^{\infty}\sum_{s=0}^{\infty}\sum_{t=0}^{\infty}\frac{k_0^2\vec{E}_{rst}(\vec{r})\vec{E}_{rst}(\vec{r}_o)}{k_{rst}^2(k_{rst}^2 - k_0^2)}, \tag{5.11}$$

where $\vec{E}_{rst}(\vec{r})$ and $\vec{E}_{rst}(\vec{r}_o)$ are the solenoidal eigenvectors of a cavity. This Green's function contains the resonances of the closed region and the function is finite at the source coordinates. At this point the Green's dyadic $\bar{\bar{G}}_e^{\mathrm{I}}$ can be written as

$$\begin{aligned}\bar{\bar{G}}_e^{\mathrm{I}}(\vec{r},\vec{r}_o) &= \bar{\bar{G}}_1(\vec{r},\vec{r}_o)+\bar{\bar{G}}_2(\vec{r},\vec{r}_o)+\bar{\bar{G}}_3(\vec{r},\vec{r}_o)\\ &= -\frac{1}{k_0^2}\nabla\nabla_o g(\vec{r},\vec{r}_o)+\frac{1}{8\pi R}\left(\bar{\bar{I}}+\frac{(\vec{r}-\vec{r}_o)(\vec{r}-\vec{r}_o)}{R^2}\right)+\bar{\bar{G}}_{2o}(\vec{r},\vec{r}_o)\\ &\quad+\sum_{r=0}^{\infty}\sum_{s=0}^{\infty}\sum_{t=0}^{\infty}\frac{k_0^2\vec{E}(\vec{r})\vec{E}(\vec{r}_o)}{k_{rst}^2(k_{rst}^2-k_0^2)}.\end{aligned} \tag{5.12}$$

Bressan and Conciauro [19], [20], [8] have calculated the three dyadics $\bar{\bar{G}}_1$, $\bar{\bar{G}}_2$ and $\bar{\bar{G}}_3$ for a three dimensional spherical cavity, a two dimensional circular resonator and a two dimensional rectangular resonator. In the next sections the three dyadics will be calculated for a three dimensional rectangular box cavity. As mentioned earlier, only the singularity extraction of the functions G_{exx}^{I} and G_{eyx}^{I} will be considered.

5.3 Calculation of the irrotational dyadic $\bar{\bar{G}}_{\mathrm{I}}$

The Green's dyadic $\bar{\bar{G}}_{\mathrm{I}}$, which contains the dominant singularity, can be expressed as

$$\bar{\bar{G}}_{\mathrm{I}}(\vec{r},\vec{r}_o) = -\frac{1}{k_0^2}\nabla\nabla_o g(\vec{r},\vec{r}_o). \tag{5.13}$$

This function $\bar{\bar{G}}_{\mathrm{I}}$ represents a low frequency approximation of the electromagnetic field in the cavity. The scalar Green's function g is given by

$$\begin{aligned}&\nabla^2 g(\vec{r},\vec{r}_o) = -\delta(\vec{r}-\vec{r}_o) && \text{in V},\\ &g = 0 && \text{at S}.\end{aligned} \tag{5.14}$$

This differential equation will be solved by using the method of images. The method of images is described in many textbooks (e.g. [21]). Using this method, the original geometry is translated into an equivalent configuration. In order to find the solution of the differential equation in the internal volume of the cavity, the boundary will be replaced with images of the point source. The solution is now only valid in the region of interest. The images plus the original source must satisfy the boundary condition at the surface S. The equivalent problem at the plane $z = 0$ is drawn in figure 5.1.
The scalar Green's function g consists of an infinite summation of the free space Green's function at the image coordinates. The sign of the Green's function changes with each image source, because the tangential electric field at the boundaries must be zero. The function g is given by

$$g(\vec{r},\vec{r}_o) = \frac{1}{4\pi}\sum_{m=-\infty}^{\infty}\sum_{n=-\infty}^{\infty}\sum_{l=-\infty}^{\infty}\frac{(-1)^{m+n+l}}{R_{mnl}}. \tag{5.15}$$

The distance between the observation points and the image sources are given by

$$R_{mnl} = \sqrt{(x-x_m)^2+(y-y_n)^2+(z-z_l)^2}. \tag{5.16}$$

The coordinates of the original source and the image sources can be expressed as

$$\begin{aligned}x_m &= (m+\tfrac{1}{2})a+(-1)^m(x_o-\tfrac{a}{2}),\\ y_n &= (n+\tfrac{1}{2})b+(-1)^n(y_o-\tfrac{b}{2}),\\ z_l &= (l+\tfrac{1}{2})c+(-1)^l(z_o-\tfrac{c}{2}).\end{aligned} \tag{5.17}$$

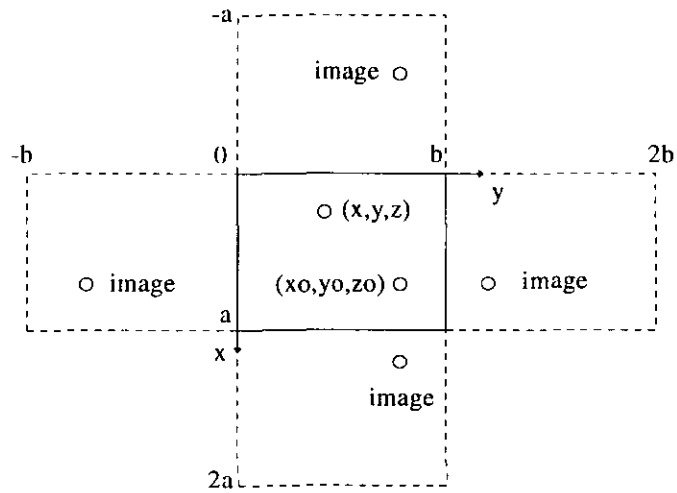

Figure 5.1: *Equivalent sources*

Note that the term R_{000} of the scalar Green's function is singular at the source coordinates. Thus the Green's dyadic $\bar{\bar{G}}_1$ can be written as a combination of a singular and a regular part

$$\begin{aligned}\bar{\bar{G}}_1(\vec{r},\vec{r}_o) &= -\frac{1}{k_0^2}\nabla\nabla_o\frac{1}{4\pi R_{000}} \\ &\quad -\frac{1}{k_0^2}\nabla\nabla_o\sum_{m=-\infty}^{\infty}\sum_{n=-\infty}^{\infty}\sum_{l=-\infty}^{\infty}\frac{(-1)^{m+n+l}}{4\pi R_{mnl}} \qquad (m,n,l)\neq(0,0,0).\end{aligned} \tag{5.18}$$

As mentioned earlier, the longitudinal components of the Green's dyadic have equal symmetry properties. This is also true for the transverse components of the Green's dyadic, therefore only two components (G_{1xx} and G_{1yx}) of the dyadic $\bar{\bar{G}}_1$ will be calculated.

5.3.1 Calculation of G_{1xx}

The dyadic G_{1xx} contains a singularity like $\frac{1}{R^3}$. Using earlier obtained results, the Green's function G_{1xx} can be written as

$$G_{1xx} = -\frac{1}{k_0^2}\frac{\partial^2}{\partial_x\partial_{x_o}}\sum_{m=-\infty}^{\infty}\sum_{n=-\infty}^{\infty}\sum_{l=-\infty}^{\infty}\frac{(-1)^{m+n+l}}{4\pi R_{mnl}}. \tag{5.19}$$

Performing some elementary calculus yields

$$\begin{aligned}G_{1xx} &= \frac{3}{4\pi k_0^2}\sum_{m=-\infty}^{\infty}\sum_{n=-\infty}^{\infty}\sum_{l=-\infty}^{\infty}\frac{(-1)^{2m+n+l}(x-x_m)^2}{R_{mnl}^5} \\ &\quad -\frac{1}{4\pi k_0^2}\sum_{m=-\infty}^{\infty}\sum_{n=-\infty}^{\infty}\sum_{l=-\infty}^{\infty}\frac{(-1)^{2m+n+l}}{R_{mnl}^3}.\end{aligned} \tag{5.20}$$

This function consists of a triple series and the singular term is given by the term $(m,n,l)=(0,0,0)$. The numerical convergence behaviour of these series will be evaluated in chapter 6.

5.3.2 Calculation of G_{1yx}

The Green's function G_{1yx} can be written as

$$G_{1yx} = -\frac{1}{k_0^2}\frac{\partial^2}{\partial_y \partial_{x_o}} \sum_{m=-\infty}^{\infty}\sum_{n=-\infty}^{\infty}\sum_{l=-\infty}^{\infty} \frac{(-1)^{m+n+l}}{4\pi R_{mnl}}. \tag{5.21}$$

Performing the term-by-term differentiations results in

$$G_{1yx} = \frac{3}{4\pi k_0^2} \sum_{m=-\infty}^{\infty}\sum_{n=-\infty}^{\infty}\sum_{l=-\infty}^{\infty} \frac{(-1)^{2m+n+l}(x-x_m)(y-y_n)}{R_{mnl}^5}. \tag{5.22}$$

5.4 Calculation of the solenoidal dyadic $\bar{\bar{G}}_2$

It has been noted in section 5.2 that the solenoidal dyadic $\bar{\bar{G}}_2$ can be obtained by using equations (5.5) and (5.6). In order to simplify the necessary calculations, we shall use a different approach in this report. The modal expansion of the electromagnetic field in a rectangular box cavity is given in chapter three. We shall use this result to obtain expressions for the dyadics $\bar{\bar{G}}_2$ and $\bar{\bar{G}}_3$. The two dyadics depend each different on the wavenumber k_0. Using (5.4) , the dyadic $\bar{\bar{G}}_2$ can be obtained by

$$\bar{\bar{G}}_2 = \lim_{k_0 \to 0} \frac{\partial^2}{\partial (k_0^2)} (k_0^2 \bar{\bar{G}}_e^{\mathrm{I}}). \tag{5.23}$$

Using (5.23), it's not necessary to solve the set of differential equations (5.5), (5.6) and (5.7). We are now able to use the results of the eigenfunction analysis outlined in chapter three. Again, only two components (G_{2xx} and G_{2yx}) will be calculated. These components consist of triple series, which can be reduced to double series.

5.4.1 Calculation of G_{2xx}

Remember that the longitudinal Green's function G^{l}_{exx} can be written as

$$\begin{aligned} G^{\mathrm{l}}_{exx}(\vec{r},\vec{r}_o) \;=\; & \sum_{r=0}^{\infty}\sum_{s=0}^{\infty}\sum_{t=0}^{\infty} \frac{4\epsilon_{or}}{abc\,(k_{rst}^2 - k_0^2)\,k_0^2} \\ & \left[k_0^2 - \left(\frac{r\pi}{a}\right)^2\right] \cos\frac{r\pi x}{a} \cos\frac{r\pi x_o}{a} \sin\frac{s\pi y}{b} \sin\frac{s\pi y_o}{b} \sin\frac{t\pi z}{c} \sin\frac{t\pi z_o}{c}. \end{aligned} \tag{5.24}$$

Using (5.23), G_{2xx} can be written as

$$\begin{aligned} G_{2xx}(\vec{r},\vec{r}_o) \;=\; & \sum_{r=0}^{\infty}\sum_{s=0}^{\infty}\sum_{t=0}^{\infty} \frac{4\epsilon_{or}\left[\left(\frac{s\pi}{b}\right)^2 + \left(\frac{t\pi}{c}\right)^2\right]}{abck_{rst}^4} \\ & \cos\frac{r\pi x}{a} \cos\frac{r\pi x_o}{a} \sin\frac{s\pi y}{b} \sin\frac{s\pi y_o}{b} \sin\frac{t\pi z}{c} \sin\frac{t\pi z_o}{c}. \end{aligned} \tag{5.25}$$

The Green's function G_{2xx} is k_0-independent. Furthermore, it is proportional to $\frac{1}{k_{rst}^4}$. It can be expected that the convergence of the series will be faster than the original series, which was proportional to $\frac{1}{k_{rst}^2 - k_0^2}$. For the case of a spherical resonator it is possible to extract the singularity in closed form [20]. Unfortunately, it is not possible to decompose the weakly singular series of a rectangular box cavity into a regular and a singular part (e.g. 5.10). So the convergence of the dyadic $\bar{\bar{G}}_2$ will be slower than the corresponding series of a spherical resonator. The function G_{2xx} is expressed as a

triple series, but it is possible to reduce one series.
Equation (5.25) can be written in the following form

$$\begin{aligned} G_{2xx} &= \frac{2a^3}{bc\pi^4}\sum_{s=0}^{\infty}\sum_{t=0}^{\infty}\left[\left(\frac{s\pi}{b}\right)^2+\left(\frac{t\pi}{c}\right)^2\right]\sin\frac{s\pi y}{b}\sin\frac{s\pi y_o}{b}\sin\frac{t\pi z}{c}\sin\frac{t\pi z_o}{c} \\ &\left[\sum_{r=0}^{\infty}\frac{\epsilon_{or}\cos r(x-x_o)\frac{\pi}{a}}{(r^2+\alpha^2)^2}+\sum_{r=0}^{\infty}\frac{\epsilon_{or}\cos r(x+x_o)\frac{\pi}{a}}{(r^2+\alpha^2)^2}\right], \end{aligned} \tag{5.26}$$

where

$$\alpha=\sqrt{\left(\frac{sa}{b}\right)^2+\left(\frac{ta}{c}\right)^2}. \tag{5.27}$$

Hansen [22] presents the following series in closed form

$$\begin{aligned} \sum_{k=0}^{\infty}\frac{\cos kx}{(k^2a^2+b^2)^2} &= \frac{1}{2b^4}+\frac{\pi}{4a^2b^3\sinh\frac{\pi b}{a}}\left[a\cosh(\pi-x)\frac{b}{a}\right. \\ &\left.+bx\sinh(\pi-x)\frac{b}{a}+\frac{\pi b}{\sinh\frac{\pi b}{a}}\cosh\frac{bx}{a}\right]. \end{aligned} \tag{5.28}$$

Using this result, the function G_{2xx} can be written as
$\underline{x \geq x_o}$

$$\begin{aligned} G_{2xx} &= \frac{a^3}{bc\pi^3}\sum_{s=0}^{\infty}\sum_{t=0}^{\infty}\frac{\left(\frac{s\pi}{b}\right)^2+\left(\frac{t\pi}{c}\right)^2}{\alpha^3\sinh\alpha\pi}\sin\frac{s\pi y}{b}\sin\frac{s\pi y_o}{b}\sin\frac{t\pi z}{c}\sin\frac{t\pi z_o}{c} \\ &\left[2\cosh\alpha(\pi-\frac{\pi}{a}x)\cosh\alpha\frac{\pi}{a}x_o\right. \\ &+2\alpha\frac{\pi}{a}x\sinh\alpha(\pi-\frac{\pi}{a}x)\cosh\alpha\frac{\pi}{a}x_o \\ &-2\alpha\frac{\pi}{a}x_o\cosh\alpha(\pi-\frac{\pi}{a}x)\sinh\alpha\frac{\pi}{a}x_o \\ &\left.+\frac{\pi\alpha}{\sinh\alpha\pi}\left[\cosh\alpha\frac{\pi}{a}(x-x_o)+\cosh\alpha\frac{\pi}{a}(x+x_o)\right]\right]. \end{aligned} \tag{5.29}$$

The symbols x and x_o have to be interchanged in the region $x < x_o$. The numerical convergence of this double series will be evaluated in chapter 6, it will be shown that the necessary computational time reduces compared to the computational time needed for the calculation of the double series presented in chapter 3. Note that the functions G_{2yy} and G_{2zz} can be calculated in a similar manner.

5.4.2 Calculation of G_{2yx}

Using (5.23), the Green's function G_{2yx} can be written as

$$\begin{aligned} G_{2yx}(\vec{r},\vec{r}_o) &= \sum_{r=0}^{\infty}\sum_{s=0}^{\infty}\sum_{t=0}^{\infty}\frac{-8rs\pi^2}{a^2b^2ck_{rst}^4} \\ &\sin\frac{r\pi x}{a}\cos\frac{r\pi x_o}{a}\cos\frac{s\pi y}{b}\sin\frac{s\pi y_o}{b}\sin\frac{t\pi z}{c}\sin\frac{t\pi z_o}{c}. \end{aligned} \tag{5.30}$$

This series can also be reduced to a double series. Using (5.28), the function G_{2yx} can be expressed as
$\underline{z \geq z_o}$

$$
\begin{aligned}
G_{2yx} = & \frac{-c^3}{a^2b^2\pi}\sum_{r=0}^{\infty}\sum_{s=0}^{\infty}\frac{rs}{\alpha^3\sinh\alpha\pi}\sin\frac{r\pi x}{a}\cos\frac{r\pi x_o}{a}\cos\frac{s\pi y}{b}\sin\frac{s\pi y_o}{b} \\
& \Big[2\sinh\alpha(\pi-\frac{\pi}{c}z)\sinh\alpha\frac{\pi}{c}z_o \\
& +2\alpha\frac{\pi}{c}z\cosh\alpha(\pi-\frac{\pi}{c}z)\sinh\alpha\frac{\pi}{c}z_o \\
& -2\alpha\frac{\pi}{c}z_o\sinh\alpha(\pi-\frac{\pi}{c}z)\cosh\alpha\frac{\pi}{c}z_o \\
& +\frac{\pi\alpha}{\sinh\alpha\pi}\left[\cosh\alpha\frac{\pi}{c}(z-z_o)-\cosh\alpha\frac{\pi}{c}(z+z_o)\right]\Big],
\end{aligned}
\tag{5.31}
$$

where

$$
\alpha=\sqrt{\left(\frac{rc}{a}\right)^2+\left(\frac{sc}{b}\right)^2}. \tag{5.32}
$$

The symbols z and z_o have to be interchanged when $z < z_o$. The other transverse components of the dyadic $\bar{\bar{G}}_2$ can be calculated in a similar manner.

5.5 Calculation of $\bar{\bar{G}}_3$

The irrotational dyadic $\bar{\bar{G}}_1$ contains the dominant singularity. This dyadic becomes important when the source and the observation coordinates are very close together. In addition, this dyadic is a low-frequency approximation of the original Green's dyadic.

The solenoidal dyadic $\bar{\bar{G}}_2$ contains the weaker singularity. This dyadic is independent of the frequency. The solenoidal dyadic $\bar{\bar{G}}_3$ will be calculated in this section. The dyadic $\bar{\bar{G}}_3$ becomes important when the wavelength is smaller than the cavity dimension (propagative effects). The dyadic $\bar{\bar{G}}_3$ is finite when the distance between the observation points and the source equals zero. $\bar{\bar{G}}_3$ will be calculated by using the following relationship

$$
\bar{\bar{G}}_3=\bar{\bar{G}}_e^1-\frac{1}{k_0^2}\lim_{k_0\to 0}(k_0^2\bar{\bar{G}}_e^1)-\lim_{k_0\to 0}\frac{\partial^2}{\partial(k_0^2)}(k_0^2\bar{\bar{G}}_e^1). \tag{5.33}
$$

Again, the two components G_{3xx} and G_{3yx} will be derived.

5.5.1 Calculation of G_{3xx}

The Green's function G_{exx}^1 is given by

$$
\begin{aligned}
G_{exx}^1(\vec{r},\vec{r}_o) = & \sum_{r=0}^{\infty}\sum_{s=0}^{\infty}\sum_{t=0}^{\infty}\frac{4\epsilon_{or}}{abc\,(k_{rst}^2-k_0^2)\,k_0^2} \\
& \left[k_0^2-\left(\frac{r\pi}{a}\right)^2\right]\cos\frac{r\pi x}{a}\cos\frac{r\pi x_o}{a}\sin\frac{s\pi y}{b}\sin\frac{s\pi y_o}{b}\sin\frac{t\pi z}{c}\sin\frac{t\pi z_o}{c}.
\end{aligned}
\tag{5.34}
$$

The function G_{3xx} can be calculated by using (5.33) and (5.34)

$$
\begin{aligned}
G_{3xx}(\vec{r},\vec{r}_o) = & \sum_{r=0}^{\infty}\sum_{s=0}^{\infty}\sum_{t=0}^{\infty}\frac{-4\epsilon_{or}k_0^2\left[\left(\frac{s\pi}{b}\right)^2+\left(\frac{t\pi}{c}\right)^2\right]}{abc(k_0^2-k_{rst}^2)k_{rst}^4} \\
& \cos\frac{r\pi x}{a}\cos\frac{r\pi x_o}{a}\sin\frac{s\pi y}{b}\sin\frac{s\pi y_o}{b}\sin\frac{t\pi z}{c}\sin\frac{t\pi z_o}{c}.
\end{aligned}
\tag{5.35}
$$

The triple series can be reduced to a double series. There are two situations

1. $\left(\frac{sa}{b}\right)^2+\left(\frac{ta}{c}\right)^2-\left(\frac{k_0a}{\pi}\right)^2\geq 0$

The function G_{3xx} is given by

$$\begin{aligned} G_{3xx} &= \frac{4k_0^2a^5}{bc\pi^6}\sum_{s=0}^{\infty}\sum_{t=0}^{\infty}\left[\left(\frac{s\pi}{b}\right)^2+\left(\frac{t\pi}{c}\right)^2\right]\sin\frac{s\pi y}{b}\sin\frac{s\pi y_o}{b}\sin\frac{t\pi z}{c}\sin\frac{t\pi z_o}{c} \\ &\quad \sum_{r=0}^{\infty}\frac{\epsilon_{or}\cos\frac{r\pi x}{a}\cos\frac{r\pi x_o}{a}}{(r^2+\alpha_1^2)(r^2+\beta^2)^2}, \end{aligned} \tag{5.36}$$

where

$$\alpha_1=\sqrt{\left(\frac{sa}{b}\right)^2+\left(\frac{ta}{c}\right)^2-\left(\frac{k_0a}{\pi}\right)^2}, \tag{5.37}$$

$$\beta=\sqrt{\left(\frac{sa}{b}\right)^2+\left(\frac{ta}{c}\right)^2}. \tag{5.38}$$

2. $\left(\frac{sa}{b}\right)^2+\left(\frac{ta}{c}\right)^2-\left(\frac{k_0a}{\pi}\right)^2<0$

$$\begin{aligned} G_{3xx} &= \frac{4k_0^2a^5}{bc\pi^6}\sum_{s=0}^{\infty}\sum_{t=0}^{\infty}\left[\left(\frac{s\pi}{b}\right)^2+\left(\frac{t\pi}{c}\right)^2\right]\sin\frac{s\pi y}{b}\sin\frac{s\pi y_o}{b}\sin\frac{t\pi z}{c}\sin\frac{t\pi z_o}{c} \\ &\quad \sum_{r=0}^{\infty}\frac{\epsilon_{or}\cos\frac{r\pi x}{a}\cos\frac{r\pi x_o}{a}}{(r^2-\alpha_2^2)(r^2+\beta^2)^2}, \end{aligned} \tag{5.39}$$

where

$$\alpha_2=\sqrt{\left(\frac{k_0a}{\pi}\right)^2-\left(\frac{sa}{b}\right)^2-\left(\frac{ta}{c}\right)^2}. \tag{5.40}$$

The last series of (5.36) and (5.39) can be written as

$$\begin{aligned} \sum_{r=0}^{\infty}\frac{\cos\frac{r\pi x}{a}\cos\frac{r\pi x_o}{a}}{(r^2\pm\alpha_{1,2}^2)(r^2+\beta^2)^2} &= \frac{\pi^4}{k_0^4a^4}\sum_{r=0}^{\infty}\frac{\cos\frac{r\pi x}{a}\cos\frac{r\pi x_o}{a}}{(r^2\pm\alpha_{1,2}^2)} \\ &\quad -\frac{\pi^4}{k_0^4a^4}\sum_{r=0}^{\infty}\frac{\cos\frac{r\pi x}{a}\cos\frac{r\pi x_o}{a}}{(r^2+\beta^2)} \\ &\quad -\frac{\pi^2}{k_0^2a^2}\sum_{r=0}^{\infty}\frac{\cos\frac{r\pi x}{a}\cos\frac{r\pi x_o}{a}}{(r^2+\beta^2)^2}. \end{aligned} \tag{5.41}$$

Using these formulae, we are able to calculate the double series representation of G_{3xx}. Again, two regions have to be distinguished.

1. $\left(\frac{sa}{b}\right)^2 + \left(\frac{ta}{c}\right)^2 - \left(\frac{k_0 a}{\pi}\right)^2 \geq 0$

Using [15], [22], the function G_{3xx} can now be expressed as

$x \geq x_o$

$$
\begin{aligned}
G_{3xx} = \sum_{s=1}^{\infty}\sum_{t=1}^{\infty} & \frac{4a\left[\left(\frac{s\pi}{b}\right)^2 + \left(\frac{t\pi}{c}\right)^2\right]}{k_0^2 \pi bc} \sin\frac{s\pi y}{b} \sin\frac{s\pi y_o}{b} \sin\frac{t\pi z}{c} \sin\frac{t\pi z_o}{c} \\
& \left[\frac{\cosh\alpha_1(\pi - \frac{\pi}{a}x)\cosh\alpha_1\frac{\pi}{a}x_o}{\alpha_1 \sinh\alpha_1\pi}\right. \\
& - \frac{\cosh\beta(\pi - \frac{\pi}{a}x)\cosh\beta\frac{\pi}{a}x_o}{\beta\sinh\beta\pi} \\
& - \frac{k_0^2 a^2}{4\pi^2\beta^3\sinh\beta\pi}\left[2\cosh\beta(\pi - \frac{\pi}{a}x)\cosh\beta\frac{\pi}{a}x_o\right. \\
& + 2\beta\frac{\pi}{a}x\sinh\beta(\pi - \frac{\pi}{a}x)\cosh\beta\frac{\pi}{a}x_o \\
& - 2\beta\frac{\pi}{a}x_o\cosh\beta(\pi - \frac{\pi}{a}x)\sinh\beta\frac{\pi}{a}x_o \\
& \left.\left. + \frac{\pi\beta}{\sinh\beta\pi}\left[\cosh\beta\frac{\pi}{a}(x - x_o) + \cosh\beta\frac{\pi}{a}(x + x_o)\right]\right]\right].
\end{aligned}
\tag{5.42}
$$

2. $\left(\frac{sa}{b}\right)^2 + \left(\frac{ta}{c}\right)^2 - \left(\frac{k_0 a}{\pi}\right)^2 < 0$

$x \geq x_o$

$$
\begin{aligned}
G_{3xx} = \sum_{s=1}^{\infty}\sum_{t=1}^{\infty} & \frac{4a\left[\left(\frac{s\pi}{b}\right)^2 + \left(\frac{t\pi}{c}\right)^2\right]}{k_0^2 \pi bc} \sin\frac{s\pi y}{b} \sin\frac{s\pi y_o}{b} \sin\frac{t\pi z}{c} \sin\frac{t\pi z_o}{c} \\
& \left[-\frac{\cos\alpha_2(\pi - \frac{\pi}{a}x)\cos\alpha_2\frac{\pi}{a}x_o}{\alpha_2 \sin\alpha_2\pi}\right. \\
& - \frac{\cosh\beta(\pi - \frac{\pi}{a}x)\cosh\beta\frac{\pi}{a}x_o}{\beta\sinh\beta\pi} \\
& - \frac{k_0^2 a^2}{4\pi^2\beta^3\sinh\beta\pi}\left[2\cosh\beta(\pi - \frac{\pi}{a}x)\cosh\beta\frac{\pi}{a}x_o\right. \\
& + 2\beta\frac{\pi}{a}x\sinh\beta(\pi - \frac{\pi}{a}x)\cosh\beta\frac{\pi}{a}x_o \\
& - 2\beta\frac{\pi}{a}x_o\cosh\beta(\pi - \frac{\pi}{a}x)\sinh\beta\frac{\pi}{a}x_o \\
& \left.\left. + \frac{\pi\beta}{\sinh\beta\pi}\left[\cosh\beta\frac{\pi}{a}(x - x_o) + \cosh\beta\frac{\pi}{a}(x + x_o)\right]\right]\right].
\end{aligned}
\tag{5.43}
$$

The symbols x and x_o have to be interchanged in the region $x < x_o$. The convergence properties of this double series will be evaluated in chapter 6. The longitudinal components G_{3yy} and G_{3zz} can be calculated in a similar manner.

5.5.2 Calculation of G_{3yx}

The Green's function G^{1}_{eyx} is given by (3.10)

$$G^{1}_{eyx} = \sum_{r=0}^{\infty}\sum_{s=0}^{\infty}\sum_{t=0}^{\infty} \frac{-8rs\pi^2}{a^2b^2ck_0^2(k_{rst}^2 - k_0^2)} \sin\frac{r\pi x}{a}\cos\frac{r\pi x_o}{a}\cos\frac{s\pi y}{b}\sin\frac{s\pi y_o}{b}\sin\frac{t\pi z}{c}\sin\frac{t\pi z_o}{c}. \tag{5.44}$$

Using (3.10) and (5.33), the function G_{3yx} can be written as

$$G_{3yx} = \sum_{r=0}^{\infty}\sum_{s=0}^{\infty}\sum_{t=0}^{\infty} \frac{-8rs\pi^2k_0^2}{a^2b^2c(k_{rst}^2 - k_0^2)k_{rst}^4} \sin\frac{r\pi x}{a}\cos\frac{r\pi x_o}{a}\cos\frac{s\pi y}{b}\sin\frac{s\pi y_o}{b}\sin\frac{t\pi z}{c}\sin\frac{t\pi z_o}{c}. \tag{5.45}$$

The triple series can also be reduced into a double series. Therefore the function G_{3yx} is written in the following form

1. $\left(\frac{rc}{a}\right)^2 + \left(\frac{sc}{b}\right)^2 - \left(\frac{k_0c}{\pi}\right)^2 \geq 0$

$$G_{3yx} = \frac{-8k_0^2c^5}{a^2b^2\pi^4}\sum_{r=0}^{\infty}\sum_{s=0}^{\infty} rs\sin\frac{r\pi x}{a}\cos\frac{r\pi x_o}{a}\cos\frac{s\pi y}{b}\sin\frac{s\pi y_o}{b} \sum_{t=0}^{\infty}\frac{\sin\frac{t\pi z}{c}\sin\frac{t\pi z_o}{c}}{(t^2+\alpha_1^2)(t^2+\beta^2)^2}. \tag{5.46}$$

2. $\left(\frac{rc}{a}\right)^2 + \left(\frac{sc}{b}\right)^2 - \left(\frac{k_0c}{\pi}\right)^2 < 0$

$$G_{3yx} = \frac{-8k_0^2c^5}{a^2b^2\pi^4}\sum_{r=0}^{\infty}\sum_{s=0}^{\infty} rs\sin\frac{r\pi x}{a}\cos\frac{r\pi x_o}{a}\cos\frac{s\pi y}{b}\sin\frac{s\pi y_o}{b} \sum_{t=0}^{\infty}\frac{\sin\frac{t\pi z}{c}\sin\frac{t\pi z_o}{c}}{(t^2-\alpha_2^2)(t^2+\beta^2)^2}, \tag{5.47}$$

where

$$\alpha_1 = \sqrt{\left(\frac{rc}{a}\right)^2 + \left(\frac{sc}{b}\right)^2 - \left(\frac{k_0c}{\pi}\right)^2}, \tag{5.48}$$

$$\alpha_2 = \sqrt{\left(\frac{k_0c}{\pi}\right)^2 - \left(\frac{rc}{a}\right)^2 - \left(\frac{sc}{b}\right)^2}, \tag{5.49}$$

$$\beta = \sqrt{\left(\frac{rc}{a}\right)^2 + \left(\frac{sc}{b}\right)^2}. \tag{5.50}$$

The last series can be written as

$$\sum_{t=0}^{\infty}\frac{\sin\frac{t\pi z}{c}\sin\frac{t\pi z_o}{c}}{(t^2 \pm \alpha_{1,2}^2)(t^2+\beta^2)^2} = \frac{\pi^4}{k_0^4c^4}\sum_{t=0}^{\infty}\frac{\sin\frac{t\pi z}{c}\sin\frac{t\pi z_o}{c}}{(t^2 \pm \alpha_{1,2}^2)} - \frac{\pi^4}{k_0^4c^4}\sum_{t=0}^{\infty}\frac{\sin\frac{t\pi z}{c}\sin\frac{t\pi z_o}{c}}{(t^2+\beta^2)} - \frac{\pi^2}{k_0^2c^2}\sum_{t=0}^{\infty}\frac{\sin\frac{t\pi z}{c}\sin\frac{t\pi z_o}{c}}{(t^2+\beta^2)^2}. \tag{5.51}$$

The function G_{3yx} can now be expressed as

1. $\left(\frac{rc}{a}\right)^2 + \left(\frac{sc}{b}\right)^2 - \left(\frac{k_0 c}{\pi}\right)^2 \geq 0$

$z \geq z_o$

$$
\begin{aligned}
G_{3yx} = & \sum_{r=1}^{\infty}\sum_{s=1}^{\infty} \frac{-4rsc\pi}{k_0^2 a^2 b^2} \cos\frac{r\pi x}{a} \sin\frac{r\pi x_o}{a} \sin\frac{s\pi y}{b} \cos\frac{s\pi y_o}{b} \\
& \left[\frac{\sinh\alpha_1(\pi - \frac{\pi}{c}z)\sinh\alpha_1\frac{\pi}{c}z_o}{\alpha_1 \sinh\alpha_1\pi} \right. \\
& - \frac{\sinh\beta(\pi - \frac{\pi}{c}z)\sinh\beta\frac{\pi}{c}z_o}{\beta\sinh\beta\pi} \\
& - \frac{k_0^4 c^2}{4\pi^2\beta^3\sinh\beta\pi} \left[2\sinh\beta(\pi - \frac{\pi}{c}z)\sinh\beta\frac{\pi}{c}z_o \right. \\
& + 2\beta\frac{\pi}{c}z\cosh\beta(\pi - \frac{\pi}{c}z)\sinh\beta\frac{\pi}{c}z_o \\
& - 2\beta\frac{\pi}{c}z_o\sinh\beta(\pi - \frac{\pi}{c}z)\cosh\beta\frac{\pi}{c}z_o \\
& \left. \left. + \frac{\pi\beta}{\sinh\beta\pi}\left[\cosh\beta\frac{\pi}{c}(z - z_o) - \cosh\beta\frac{\pi}{c}(z + z_o)\right]\right]\right].
\end{aligned}
\tag{5.52}
$$

2. $\left(\frac{rc}{a}\right)^2 + \left(\frac{sc}{b}\right)^2 - \left(\frac{k_0 c}{\pi}\right)^2 < 0$

$z \geq z_o$

$$
\begin{aligned}
G_{3yx} = & \sum_{r=1}^{\infty}\sum_{s=1}^{\infty} \frac{-4rsc\pi}{k_0^2 a^2 b^2} \cos\frac{r\pi x}{a} \sin\frac{r\pi x_o}{a} \sin\frac{s\pi y}{b} \cos\frac{s\pi y_o}{b} \\
& \left[\frac{\sin\alpha_2(\pi - \frac{\pi}{c}z)\sin\alpha_2\frac{\pi}{c}z_o}{\alpha_2 \sin\alpha_2\pi} \right. \\
& - \frac{\sinh\beta(\pi - \frac{\pi}{c}z)\sinh\beta\frac{\pi}{c}z_o}{\beta\sinh\beta\pi} \\
& - \frac{k_0^4 c^2}{4\pi^2\beta^3\sinh\beta\pi} \left[2\sinh\beta(\pi - \frac{\pi}{c}z)\sinh\beta\frac{\pi}{c}z_o \right. \\
& + 2\beta\frac{\pi}{c}z\cosh\beta(\pi - \frac{\pi}{c}z)\sinh\beta\frac{\pi}{c}z_o \\
& - 2\beta\frac{\pi}{c}z_o\sinh\beta(\pi - \frac{\pi}{c}z)\cosh\beta\frac{\pi}{c}z_o \\
& \left. \left. + \frac{\pi\beta}{\sinh\beta\pi}\left[\cosh\beta\frac{\pi}{c}(z - z_o) - \cosh\beta\frac{\pi}{c}(z + z_o)\right]\right]\right].
\end{aligned}
\tag{5.53}
$$

The symbols z and z_o have to be interchanged when $z < z_o$.

5.6 Conclusions

It is shown in chapter four that the Green's functions are slowly convergent when the observation coordinates are very close to the source coordinates. In this chapter, we have used the fact that the singularity of the Green's function for a rectangular cavity is essentially the same as the singularity

of the free space Green's function. The Green's function is decomposed into three parts: $\bar{\bar{G}}_1$, $\bar{\bar{G}}_2$ and $\bar{\bar{G}}_3$. These three Green's dyadics are related to each other by three partial differential equations. Solving these equations is a tedious process, therefore we will use another approach. The dyadics depend each differently on the wavenumber k_o, this knowledge will be used when calculating the Green's functions. The dyadic $\bar{\bar{G}}_1$ contains the dominant singularity ($\frac{1}{R^3}$) and this dyadic is a low frequency approximation of the original Green's dyadic. This dyadic has been expressed as a triple series.

The dyadic $\bar{\bar{G}}_2$ contains the weaker singularity ($\frac{1}{R}$), this dyadic is independent of the wavenumber k_0. This dyadic can be expressed as a double series.

The dyadic $\bar{\bar{G}}_3$ is finite at the source coordinates and contains the resonances of the cavity. It becomes important when the wavelength is much smaller than the cavity dimensions. This dyadic has also been expressed as a double series.

The numerical convergence properties of these series compared to the non decomposed Green's dyadic will be evaluated in the next chapter.

Chapter 6

Numerical results of the Green's functions using singularity extraction

6.1 Introduction

In this chapter the convergence properties of the decomposed Green's functions (chapter 5) will be compared to the original Green's functions. The partial sums of the series will be evaluated to make an appraisal of the convergence properties for the two different types of Green's functions. Similar to the analysis in chapter five, only two components G^{1}_{exx} and G^{1}_{eyx} will be calculated. Three regions will be considered when comparing the two types of Green's functions.

- Region 1. The distance between the source point and observation point is large
- Region 2. The observation point is very close to the source
- Region 3. The observation point is in the vicinity of the source, but not so near as region 2, we will call this area the 'intermediate region'

It will be shown that the convergence properties of the two representations of the Green's functions are equal in region 1. In region 2, the convergence of the decomposed Green's function is much faster that the original function. The convergence of the decomposed series in region 3 is faster than the convergence of the original series, but the convergence is still slow.

6.2 Large distance between source and observation point

We shall compare the convergence properties between the two representations for the Green's functions in this section. The first Green's function $\bar{\bar{G}}^{1}_{e}$ is calculated in chapter three and the second decomposed Green's function is calculated in chapter five.

The series representing the Green's functions are too complicated to permit a simple analysis of their converging properties. Therefore we shall not evaluate the convergence properties in a mathematical sense. Our discussion is based on a numerical analysis of the two types of Green's functions. Therefore the partial sums of the triple or double series will be calculated. These partial sums have the following form

$$S_n = \sum_{r=0}^{n} \sum_{s=0}^{n} f(r,s) \tag{6.1}$$

where S_n denotes the partial sum. The above formula can also be calculated for the case of a triple series

$$S_n = \sum_{r=0}^{n}\sum_{s=0}^{n}\sum_{t=0}^{n} f(r,s,t) \tag{6.2}$$

The original Green's function will be calculated by using a double series representation. The decomposed Green's function can be written in the following form

$$\bar{\bar{G}}_e^{\,l}(\vec{r},\vec{r}_o) = \bar{\bar{G}}_1(\vec{r},\vec{r}_o) + \bar{\bar{G}}_2(\vec{r},\vec{r}_o) + \bar{\bar{G}}_3(\vec{r},\vec{r}_o) \tag{6.3}$$

The dyadic $\bar{\bar{G}}_1$ will be calculated by a triple series, the other two dyadics by a double series. So the partial sums of the decomposed Green's functions can be written as

$$S_n = \sum_{r=0}^{n}\sum_{s=0}^{n}\sum_{t=0}^{n} f(r,s,t) + \sum_{r=0}^{n}\sum_{s=0}^{n} g(r,s) \tag{6.4}$$

As mentioned earlier, two components of the Green's dyadic will be calculated (G^{l}_{exx} and G^{l}_{eyx}). These Green's functions are implemented in a Fortran code. We shall evaluate the convergence properties of the Green's functions using this code. The geometry of the cavity is given by figure 3.1. The dimensions of the cavity are equal to (a, b, c) = (3.4 m, 3.7 m, 2.2 m). The frequency is 2 GHz and the source dipole is directed in the x-direction. In this section the coordinates of the source and the field point are equal to (x_o, y_o, z_o) = (1m, 1m, 1m) and (x, y, z) = (2m, 2m, 2m), respectively. First the longitudinal Green's function G_{xx} will be calculated.

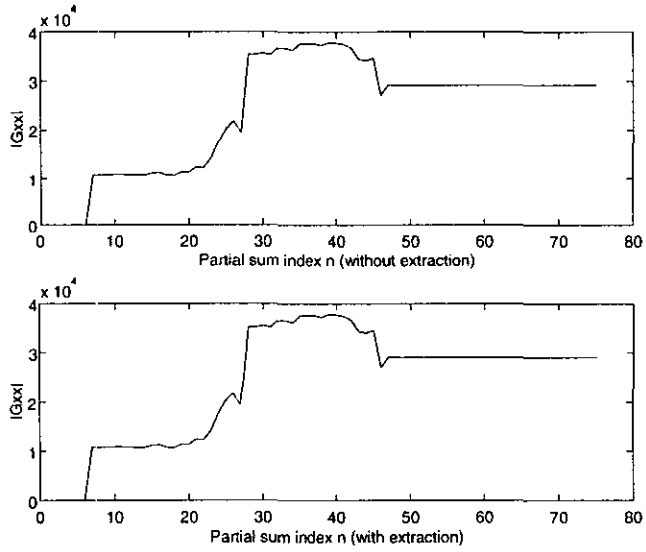

Figure 6.1: *Comparison between two representations of* G_{xx}

The convergence properties of both Green's functions appear to be equal. This is due to the fact that the distance between the observation point and the source is large. Note that the decomposed Green's function consists of more mathematical expressions (subtraction, multiplication etc.) compared to the original Green's function. So in practice the computational time used for the calculation of the decomposed Green's function will be larger than the time used for the calculation of the original function.

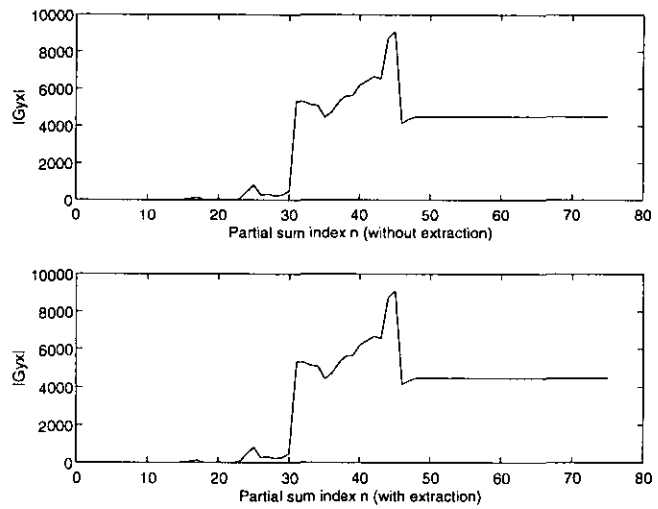

Figure 6.2: *Comparison between two representations of* G_{yx}

The convergence properties of the original transverse component G_{yx} have been compared to the decomposed Green's function in figure 6.2.

It is clear from figure 6.2 that the convergence properties of the two representations for the Green's functions G_{yx} are equal. It can be concluded that in this region (large distance between the source and the observation point), the original Green's function is the best representation for calculating the electromagnetic fields inside the cavity. Less computational time is needed for the calculation of the original Green's function compared to the decomposed Green's function.

6.3 Observation point very close to the source

In this region the dyadic $\bar{\bar{G}}_1$, which contains the dominant singularity of the order $\frac{1}{R^3}$, will be very large compared to the other dyadics. According to equation (5.18), the singularity is expressed in closed form. So it can be expected that the convergence properties of the decomposed Green's functions are better than the properties of the original Green's functions.

The position of the source is still (x_o, y_o, z_o) = (1m, 1m, 1m). First we will calculate the Green's function G_{yx}. The coordinates of the observation point are (x, y, z) = (1.005m, 1.005m, 1.005m). The two representations of the function G_{yx} are shown in figure 6.3.

Note that the two figures have different scales with respect to the vertical axis. The convergence of the original series is very slow, while the decomposed Green's function is rapidly convergent. In this case (source near observation point), the best choice is to use the decomposed Green's function for calculating the electromagnetic fields.

The same comparison between the two forms of Green's functions can be made for the component G_{xx}. The position of the source is (1 m, 1 m, 1 m) and the coordinates of the field point are (1.00000005 m, 1.00000005 m, 1.00000005 m).

These figures have also different scales with respect to the vertical axis. The best choice is to use the decomposed Green's functions for calculating the electromagnetic fields inside the cavity.

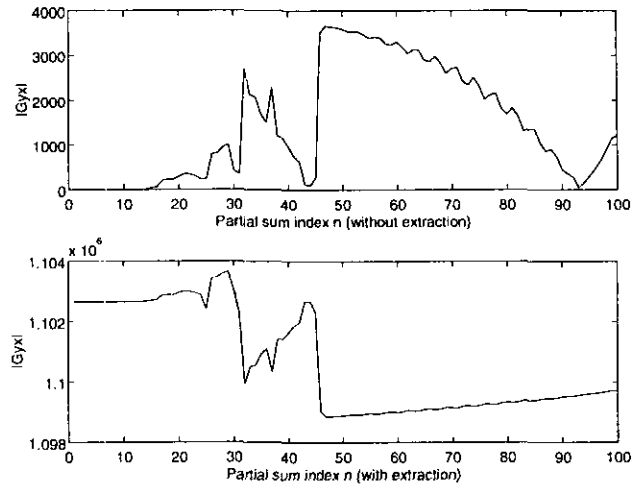

Figure 6.3: *Comparison between two representations of* G_{yx}

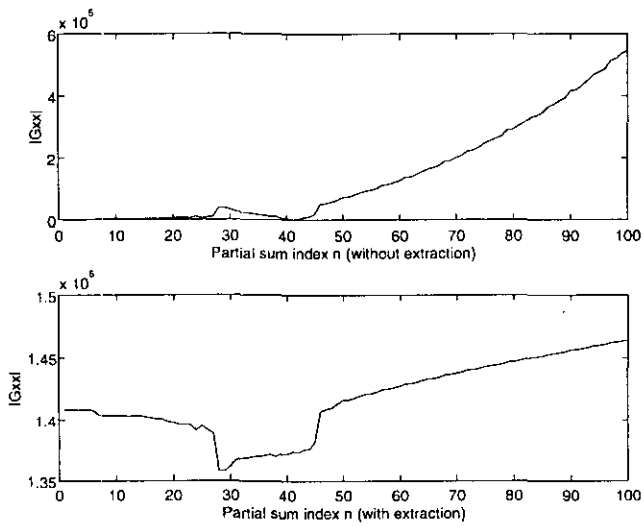

Figure 6.4: *Comparison between two representations of* G_{xx}

6.4 Numerical convergence of the Green's function in the intermediate region

In region one and two, the convergence of the decomposed Green's functions is fast. In region one, the source is far away from the observation point. So the field points, which are parameters of the Green's functions, are not in the neighbourhood of the singularity in this region. Therefore the series will converge well in this region. In region two the source is very near the observation point. The dominant singularity of the series is expressed in closed form. The series converge also well in region two. In region three, the weaker singularity (like $\frac{1}{R}$) is important. This singularity is not expressed in closed form, it can be expected that the convergence properties are not very well in this region. The convergence behaviour of the Green's function G_{yx} will be visualized in figure 6.5. The coordinates of the source are (1 m, 1 m, 1 m) and the coordinates of the field point are (1.03 m, 1.03 m, 1.03 m). The convergence of the decomposed Green's functions G_{yx} is not so fast as in the other two regions.

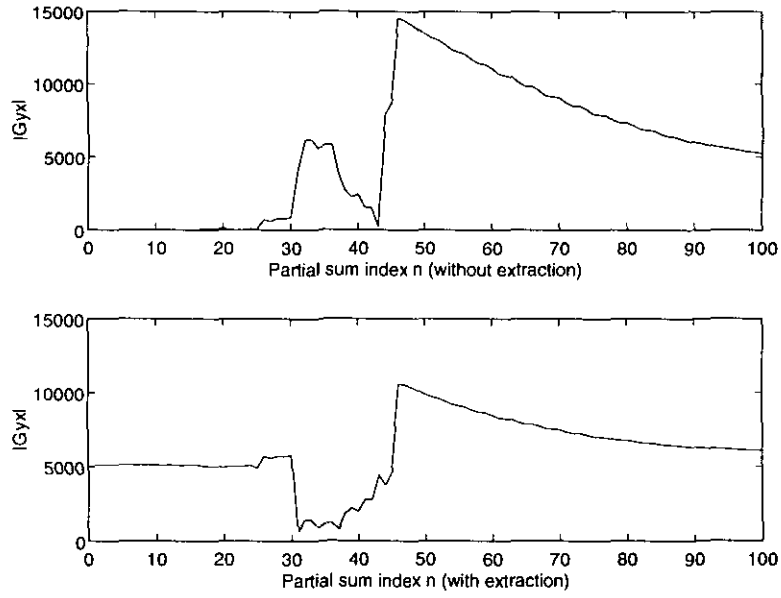

Figure 6.5: *Comparison between two representations of* G_{yx}

Nevertheless, the convergence behaviour of the decomposed Green's functions is better than the convergence properties of the original function.

The partial sums of the function G_{xx} are displayed in figure 6.6. The coordinates of the source are (1 m, 1 m, 1 m) and the coordinates of the observation point are (1.001 m, 1.001 m, 1.001 m).

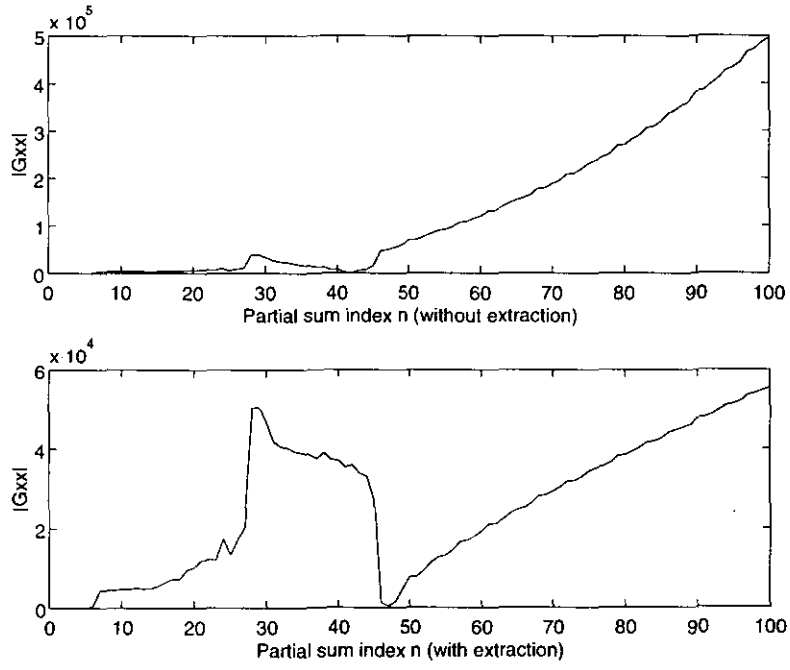

Figure 6.6: *Comparison between two representations of* G_{xx}

6.5 Conclusions

The convergence properties of the Green's functions have been improved using an extraction technique. To compare the representations with and without the extraction technique, the internal volume of the cavity has been divided into three regions.

In region 1, the distance between the observation point and source is very large. From the figures presented in section 6.2, it can be concluded that the numerical convergence of the original Green's function resembles the convergence properties of the extracted Green's function. However, in practice the computational time used for the calculation of the extracted Green's function will be larger than the time used for the calculation of the original Green's function. This is due to the fact that the decomposed Green's function consists of more mathematical expressions.

The observation point is very close to the source point in region 2. The convergence properties of the original Green's function is very slow inside this region, while the decomposed Green's function is rapidly convergent.

In the intermediate region, the observation point is in the vicinity of the source, but not so near as region 2. The convergence behaviour of the decomposed Green's function is better than the convergence properties of the original function. However, the convergence is not so fast as in the other regions.

Chapter 7

Conclusion

In order to predict the phases, strengths and polarisations of the electromagnetic fields inside an indoor environment, a deterministic model has been developed. The electromagnetic fields inside a perfectly conducting rectangular box cavity can be calculated by using the analysis presented in this report. Much attention is given to the convergence properties of various series representing the electromagnetic field. It has been shown that the electromagnetic fields are slowly convergent not only near the source, but also in some other regions inside the cavity. This depends on which series will be calculated in closed form.

Furthermore it has been shown that the convergence properties can be improved by using a so called 'extraction technique'. Especially near the source much computational time can be saved by using this extraction technique.

Finally various field distributions and polarisations inside a cavity are investigated in this report. Due to reflection of the waves against the walls a multipath environment is created. It has been shown in this report that the amplitudes of the electromagnetic fields change rapidly inside the cavity.

Appendix A

Free-space Green's functions

In chapter four the electromagnetic fields inside a cavity are compared to the electromagnetic fields in free space. The electromagnetic fields in free space are usually given in spherical coordinates in literature. We will derive in this section the electromagnetic fields caused by a z-directed electric dipole developed in rectangular coordinates. The electromagnetic field can be determined easily by using a vector potential. The vector potential A_{ez} is given by

$$A_{ez} = \frac{\mu_o}{4\pi} \frac{e^{-jk_0|\vec{r}-\vec{r}_o|}}{|\vec{r}-\vec{r}_o|} \tag{A.1}$$

The magnetic field can be calculated by using

$$\vec{H} = \frac{1}{\mu_o} \nabla \times A_{ez}\vec{e}_z \tag{A.2}$$

This will be written as

$$\vec{H} = \frac{1}{\mu_o} \frac{\partial A_{ez}}{\partial y}\vec{e}_x - \frac{1}{\mu_o} \frac{\partial A_{ez}}{\partial x}\vec{e}_y \tag{A.3}$$

Using the above equations, the magnetic field is given by

$$H_x = \frac{1}{4\pi} \left[\frac{-jk_0}{|\vec{r}-\vec{r}_o|^2} - \frac{1}{|\vec{r}-\vec{r}_o|^3} \right] (y-y_o) e^{-jk_0|\vec{r}-\vec{r}_o|} \tag{A.4}$$

$$H_y = \frac{-1}{4\pi} \left[\frac{-jk_0}{|\vec{r}-\vec{r}_o|^2} - \frac{1}{|\vec{r}-\vec{r}_o|^3} \right] (x-x_o) e^{-jk_0|\vec{r}-\vec{r}_o|} \tag{A.5}$$

$$H_z = 0 \tag{A.6}$$

The electric field can be calculated from the vector potential

$$\vec{E} = \frac{1}{j\omega\epsilon_o\mu_o} \nabla \times \nabla \times A_{ez}\vec{e}_z \tag{A.7}$$

The above equation can be written as

$$\vec{E} = \frac{-1}{j\omega\epsilon_o} \frac{\partial H_y}{\partial z}\vec{e}_x + \frac{1}{j\omega\epsilon_o} \frac{\partial H_x}{\partial z}\vec{e}_y + \frac{1}{j\omega\epsilon_o} \left[\frac{\partial H_y}{\partial x} - \frac{\partial H_x}{\partial y} \right] \vec{e}_z \tag{A.8}$$

The electric field components are given by

$$E_x = \frac{-k_0^3}{4\pi\omega\epsilon_o} \left[\frac{1}{jk_0|\vec{r}-\vec{r}_o|^3} - \frac{3}{k_0^2|\vec{r}-\vec{r}_o|^4} - \frac{3}{jk_0^3|\vec{r}-\vec{r}_o|^5} \right] (x-x_o)(z-z_o) e^{-jk_0|\vec{r}-\vec{r}_o|} \tag{A.9}$$

$$E_y = \frac{-k_0^3}{4\pi\omega\epsilon_o}\left[\frac{1}{jk_0|\vec{r}-\vec{r}_o|^3} - \frac{3}{k_0^2|\vec{r}-\vec{r}_o|^4} - \frac{3}{jk_0^3|\vec{r}-\vec{r}_o|^5}\right](y-y_o)(z-z_o)e^{-jk_0|\vec{r}-\vec{r}_o|} \quad \text{(A.10)}$$

$$\begin{aligned} E_z = {} & \frac{1}{2\pi\omega\epsilon_o}\left[\frac{k_0}{|\vec{r}-\vec{r}_o|^4} - \frac{j}{|\vec{r}-\vec{r}_o|^5}\right](z-z_o)^2 e^{-jk_0|\vec{r}-\vec{r}_o|} \\ & + \frac{1}{4\pi\omega\epsilon_o}\left[\frac{-jk_0^2}{|\vec{r}-\vec{r}_o|^3} - \frac{k_0}{|\vec{r}-\vec{r}_o|^4} + \frac{j}{|\vec{r}-\vec{r}_o|^5}\right]\left[(x-x_o)^2 + (y-y_o)^2\right] e^{-jk_0|\vec{r}-\vec{r}_o|} \end{aligned} \quad \text{(A.11)}$$

References

[1] Hashemi, H.
THE INDOOR RADIO PROPAGATION CHANNEL.
Proceedings of the IEEE, Vol. 81 (1993), p. 943-968.

[2] Fujimoto, K.
OVERVIEW OF ANTENNA SYSTEMS FOR MOBILE COMMUNICATIONS AND PROSPECTS FOR THE FUTURE TECHNOLOGY.
IEICE Transactions, Vol. E74 (1991), p. 3191-3201.

[3] Tai, C.T. and P. Rozenfeld
DIFFERENT REPRESENTATIONS OF DYADIC GREEN'S FUNCTIONS FOR A RECTANGULAR CAVITY.
IEEE Trans. on Microwave Theory and Techn., Vol. MTT-24 (1976), p. 597-601.

[4] Collin, R.E.
FIELD THEORY OF GUIDED WAVES.
Piscataway: IEEE Press, 1990.

[5] Collin, R.E.
ON THE INCOMPLETENESS OF E AND H MODES IN WAVE GUIDES.
Can. J. Phys., Vol. 51 (1973), p. 1135-1140.

[6] Wu, D.I.
ON THE EFFECT OF A ROTATING SCATTERER IN AN OVER-MODED RECTANGULAR CAVITY.
Ph.D. dissertation, Univ. of Colorado, Boulder, May 1987.

[7] Stratton, J.
ELECTROMAGNETIC THEORY.
New York: McGraw-Hill, 1941.

[8] Bressan, M. and G. Conciauro
RAPIDLY CONVERGING EXPRESSIONS FOR DYADIC GREEN'S FUNCTIONS IN TWO-DIMENSIONAL RESONATORS OF CIRCULAR AND RECTANGULAR CROSS-SECTION.
Alta Frequenza, Vol. LII (1983), p. 188-190.

[9] Bladel, J. van
SINGULAR ELECTROMAGNETIC FIELDS AND SOURCES.
Oxford: Clarendon Press, 1991.

[10] Stinson, D.C.
INTERMEDIATE MATHEMATICS OF ELECTROMAGNETICS.
New Jersey: Prentice-Hall, 1976.

[11] Ghose, R.N.
MICROWAVE CIRCUIT THEORY AND ANALYSIS.
New York: McGraw-Hill, 1961.

[12] Yaghjian, A.D.
ELECTRIC DYADIC GREEN'S FUNCTIONS IN THE SOURCE REGION.
Proc. of the IEEE, Vol. 68 (1980), p. 248-263.

[13] Omar, A.S. and E. Jensen, S. Lutgert
ON THE MODAL EXPANSION OF RESONATOR FIELD IN THE SOURCE REGION.
IEEE Trans. on Microwave Theory and Techn., Vol. MTT-40 (1992), p. 1730-1732.

[14] Johnson, W.A. and A.Q. Howard, D.G. Dudley
ON THE IRROTATIONAL COMPONENT OF THE ELECTRIC GREEN'S DYADIC.
Radio Science, Vol. 14 (1979), p. 961-967.

[15] Gradshteyn, I.S. and I.M. Ryzhik
TABLE OF INTEGRALS SERIES AND PRODUCTS.
New York: Academic Press, 1965.

[16] Lo, T. and J. Litva
ANGLES OF ARRIVAL OF INDOOR MULTIPATH.
Electronics Letters, Vol. 28 (1992), p. 1687-1689.

[17] Howard, A.Q. and D.B. Seidel
SINGULARITY EXTRACTION IN KERNEL FUNCTIONS IN CLOSED REGIONS.
Radio Science, Vol. 13 (1978), p. 425-429.

[18] Daniele, V. and M. Orefice
DYADIC GREEN'S FUNCTIONS IN BOUNDED MEDIA.
IEEE Trans. on Antennas and Prop., Vol. AP-32 (1984), p. 193-196.

[19] Bressan, M. and G. Conciauro
SINGULARITY EXTRACTION FROM THE ELECTRIC GREEN'S FUNCTION FOR A SPHERICAL RESONATOR.
IEEE Trans. on Microwave Theory and Tech., Vol. MTT-33 (1985), p. 407-414.

[20] Bressan, M. and G. Conciauro
RAPIDLY CONVERGING EXPRESSIONS OF ELECTRIC DYADIC GREEN'S FUNCTIONS FOR RESONATORS.
In: Proc. URSI Symp. on Electromagnetic Theory, Santiago de Compostella (Spain) 23-26 August 1983.
P. 41-44.

[21] Kong, J.A.
ELECTROMAGNETIC WAVE THEORY.
New York: Wiley, 1986.

[22] Hansen, E.R.
A TABLE OF SERIES AND PRODUCTS.
New Jersey: Prentice-Hall, 1975, p. 243.

Eindhoven University of Technology Research Reports ISSN 0167-9708
Coden: TEUEDE

Faculty of Electrical Engineering

(260) Rooijackers, J.E.
ALGORITHMS FOR SPEECH CODING SYSTEMS BASED ON LINEAR PREDICTION.
EUT Report 92-E-260. 1992. ISBN 90-6144-260-5

(261) Boom, T.J.J. van den and A.A.H. Damen, Martin Klompstra
IDENTIFICATION FOR ROBUST CONTROL USING AN H-infinity NORM.
EUT Report 92-E-261. 1992. ISBN 90-6144-261-3

(262) Groten, M. and W. van Etten
LASER LINEWIDTH MEASUREMENT IN THE PRESENCE OF RIN AND USING THE RECIRCULATING SELF HETERODYNE METHOD.
EUT Report 92-E-262. 1992. ISBN 90-6144-262-1

(263) Smolders, A.B.
RIGOROUS ANALYSIS OF THICK MICROSTRIP ANTENNAS AND WIRE ANTENNAS EMBEDDED IN A SUBSTRATE.
EUT Report 92-E-263. 1992. ISBN 90-6144-263-X

(264) Freriks, L.W. and P.J.M. Cluitmans, M.J. van Gils
THE ADAPTIVE RESONANCE THEORY NETWORK: (Clustering-) behaviour in relation with brainstem auditory evoked potential patterns.
EUT Report 92-E-264. 1992. ISBN 90-6144-264-8

(265) Wellen, J.S. and F. Karouta, M.F.C. Schemmann, E. Smalbrugge, L.M.F. Kaufmann
MANUFACTURING AND CHARACTERIZATION OF GAAS/ALGAAS MULTIPLE QUANTUMWELL RIDGE WAVEGUIDE LASERS.
EUT Report 92-E-265. 1992. ISBN 90-6144-265-6

(266) Cluitmans, L.J.M.
USING GENETIC ALGORITHMS FOR SCHEDULING DATA FLOW GRAPHS.
EUT Report 92-E-266. 1992. ISBN 90-6144-266-4

(267) Józwiak, L. and A.P.H. van Dijk
A METHOD FOR GENERAL SIMULTANEOUS FULL DECOMPOSITION OF SEQUENTIAL MACHINES: Algorithms and implementation.
EUT Report 92-E-267 1992. ISBN 90-6144-267-2

(268) Boom, H. van den and W. van Etten, W.H.C. de Krom, P. van Bennekom, F. Huijskens, L. Niessen, F. de Leijer
AN OPTICAL ASK AND FSK PHASE DIVERSITY TRANSMISSION SYSTEM.
EUT Report 92-E-268. 1992. ISBN 90-6144-268-0

(269) Putten, P.H.A. van der
MULTIDISCIPLINAIR SPECIFICEREN EN ONTWERPEN VAN MICROELEKTRONICA IN PRODUKTEN (in Dutch).
EUT Report 93-E-269. 1993. ISBN 90-6144-269-9

(270) Bloks, R.H.J.
PROGRIL: A language for the definition of protocol grammars.
EUT Report 93-E-270. 1993. ISBN 90-6144-270-2

(271) Bloks, R.H.J.
CODE GENERATION FOR THE ATTRIBUTE EVALUATOR OF THE PROTOCOL ENGINE GRAMMAR PROCESSOR UNIT.
EUT Report 93-E-271. 1993. ISBN 90-6144-271-0

(272) Yan, Keping and E.M. van Veldhuizen
FLUE GAS CLEANING BY PULSE CORONA STREAMER.
EUT Report 93-E-272. 1993. ISBN 90-6144-272-9

Eindhoven University of Technology Research Reports ISSN 0167-9708
Coden: TEUEDE

Faculty of Electrical Engineering

(273) Smolders, A.B.
FINITE STACKED MICROSTRIP ARRAYS WITH THICK SUBSTRATES.
EUT Report 93-E-273. 1993. ISBN 90-6144-273-7

(274) Bollen, M.H.J. and M.A. van Houten
ON INSULAR POWER SYSTEMS: Drawing up an inventory of phenomena and research possibilities.
EUT Report 93-E-274. 1993. ISBN 90-6144-274-5

(275) Deursen, A.P.J. van
ELECTROMAGNETIC COMPATIBILITY: Part 5, installation and mitigation guidelines, section 3, cabling and wiring.
EUT Report 93-E-275. 1993. ISBN 90-6144-275-3

(276) Bollen, M.H.J.
LITERATURE SEARCH FOR RELIABILITY DATA OF COMPONENTS IN ELECTRIC DISTRIBUTION NETWORKS.
EUT Report 93-E-276. 1993. ISBN 90-6144-276-1

(277) Weiland, Siep
A BEHAVIORAL APPROACH TO BALANCED REPRESENTATIONS OF DYNAMICAL SYSTEMS.
EUT Report 93-E-277. 1993. ISBN 90-6144-277-X

(278) Gorshkov, Yu.A. and V.I. Vladimirov
LINE REVERSAL GAS FLOW TEMPERATURE MEASUREMENTS: Evaluations of the optical arrangements for the instrument.
EUT Report 93-E-278. 1993. ISBN 90-6144-278-8

(279) Creyghton, Y.L.M. and W.R. Rutgers, E.M. van Veldhuizen
IN-SITU INVESTIGATION OF PULSED CORONA DISCHARGE.
EUT Report 93-E-279. 1993. ISBN 90-6144-279-6

(280) Li, H.Q. and R.P.P. Smeets
GAP-LENGTH DEPENDENT PHENOMENA OF HIGH-FREQUENCY VACUUM ARCS.
EUT Report 93-E-280. 1993. ISBN 90-6144-280-X

(281) Di, Chennian and Jochen A.G. Jess
ON THE DEVELOPMENT OF A FAST AND ACCURATE BRIDGING FAULT SIMULATOR.
EUT Report 94-E-281. 1994. ISBN 90-6144-281-8

(282) Falkus, H.M. and A.A.H. Damen
MULTIVARIABLE H-INFINITY CONTROL DESIGN TOOLBOX: User manual.
EUT Report 94-E-282. 1994. ISBN 90-6144-282-6

(283) Meng, X.Z. and J.G.J. Sloot
THERMAL BUCKLING BEHAVIOUR OF FUSE WIRES.
EUT Report 94-E-283. 1994. ISBN 90-6144-283-4

(284) Rangelrooij, A. van and J.P.M. Voeten
CCSTOOL2: An expansion, minimization, and verification tool for finite state CCS descriptions.
EUT Report 94-E-284. 1994. ISBN 90-6144-284-2

(285) Roer, Th.G. van de
MODELING OF DOUBLE BARRIER RESONANT TUNNELING DIODES: D.C. and noise model.
EUT Report 95-E-285. 1995. ISBN 90-6144-285-0

(286) Dolmans, G.
ELECTROMAGNETIC FIELDS INSIDE A LARGE ROOM WITH PERFECTLY CONDUCTING WALLS.
EUT Report 95-E-286. 1995. ISBN 90-6144-286-9